INTERNATIONAL STANDARD

ISO 13424

First edition
2013-10-01

Surface chemical analysis — X-ray photoelectron spectroscopy — Reporting of results of thin-film analysis

Analyse chimique des surfaces — Spectroscopie de photoélectrons X — Rapport des résultats de l'analyse de films minces

Reference number
ISO 13424:2013(E)

COPYRIGHT PROTECTED DOCUMENT

ISO copyright office
Case postale 56 • CH-1211 Geneva 20
Tel. + 41 22 749 01 11
Fax + 41 22 749 09 47
E-mail copyright@iso.org
Web www.iso.org

Published in Switzerland

Contents

Page

Foreword

ISO (the International Organization for Standardization) is a worldwide federation of national standards bodies (ISO member bodies). The work of preparing International Standards is normally carried out through ISO technical committees. Each member body interested in a subject for which a technical committee has been established has the right to be represented on that committee. International organizations, governmental and non-governmental, in liaison with ISO, also take part in the work. ISO collaborates closely with the International Electrotechnical Commission (IEC) on all matters of electrotechnical standardization.

The procedures used to develop this document and those intended for its further maintenance are described in the ISO/IEC Directives, Part 1. In particular the different approval criteria needed for the different types of ISO documents should be noted. This document was drafted in accordance with the editorial rules of the ISO/IEC Directives, Part 2 (see www.iso.org/directives).

Attention is drawn to the possibility that some of the elements of this document may be the subject of patent rights. ISO shall not be held responsible for identifying any or all such patent rights. Details of any patent rights identified during the development of the document will be in the Introduction and/or on the ISO list of patent declarations received (see www.iso.org/patents).

Any trade name used in this document is information given for the convenience of users and does not constitute an endorsement.

For an explanation on the meaning of ISO specific terms and expressions related to conformity assessment, as well as information about ISO's adherence to the WTO principles in the Technical Barriers to Trade (TBT) see the following URL: Foreword - Supplementary information

The committee responsible for this document is ISO/TC 201, *Surface chemical analysis*, Subcommittee SC 7, *Electron spectroscopies*.

Introduction

X-ray photoelectron spectroscopy (XPS) is widely used for the characterization of surfaces of materials, especially for overlayer thin films on a substrate. The chemical composition of the near-surface region of a thin film can be determined by XPS. If the film has a uniform thickness and the thickness is less than about three times the mean escape depth (MED) for the measured photoelectrons, the film thickness and the depth distribution of elements or chemical states of elements in the film can be determined by angle-resolved XPS or peak-shape analysis . For thicker films, the depth distributions of elements in the film can be obtained by sputter-depth profiling. Possible lateral inhomogeneities in film thicknesses or depth profiles can be determined if the XPS system has sufficient lateral resolution. These XPS applications are particularly valuable for characterizing thin-film nanostructures since the MED is typically less than 5 nm for many materials and common XPS measurement conditions.

Clauses 6 and 7 of this International Standard provide guidance to the operator of an XPS instrument in making efficient measurements for determining meaningful chemical compositions and film thicknesses for overlayer films on a substrate. Clause 8 of this International Standard shows the information to be included in reports of the measurements and the analyses of the XPS data. Annex A, Annex B, Annex C, and Annex D provide supplementary information on methods of data analysis for different types of XPS measurements on thin-film samples.

Surface chemical analysis — X-ray photoelectron spectroscopy — Reporting of results of thin-film analysis

1 Scope

This International Standard specifies the minimum amount of information required in reports of analyses of thin films on a substrate by XPS. These analyses involve measurement of the chemical composition and thickness of homogeneous thin films, and measurement of the chemical composition as a function of depth of inhomogeneous thin films by angle-resolved XPS, XPS sputter-depth profiling, peak-shape analysis, and variable photon energy XPS.

2 Normative references

The following documents, in whole or in part, are normatively referenced in this document and are indispensable for its application. For dated references, only the edition cited applies. For undated references, the latest edition of the referenced document (including any amendments) applies.

ISO 18115-1:2010, *Surface chemical analysis — Vocabulary — Part 1: General terms and terms used in spectroscopy*

3 Terms and definitions

For the purposes of this document, the terms and definitions in ISO 18115-1:2010 apply.

4 Abbreviated terms

AES	Auger electron spectroscopy
ARXPS	Angle-resolved X-ray photoelectron spectroscopy
IMFP	Inelastic mean free path
MED	Mean escape depth
RSF	Relative sensitivity factor
TRMFP	Transport mean free path
XPS	X-ray photoelectron spectroscopy

5 Overview of thin-film analysis by XPS

5.1 Introduction

XPS analyses of thin films on substrate can provide information on the variation of chemical composition with depth and on film thicknesses. Several XPS methods can be used if the total film thickness is less than three times the largest MED for the detected photoelectrons. The MED for particular photoelectrons is a function of the IMFP and the emission angle of the photoelectrons with respect to the surface normal. The IMFP depends on the photoelectron energy and the material. MED values can be obtained from a database.[1] A simple analytical formula for estimating MEDs has been published for emission angles ≤50°.[2] For such emission angles, the MED is less than the product of the IMFP and the cosine of the

emission angle by an amount that depends on the strength of the elastic scattering of the photoelectrons in the film.[2] Both the IMFP and the strength versus depend on the chemical composition of the film. The MED is typically less than 5 nm for many materials and common XPS instruments and measurement conditions. If the effects of elastic scattering are neglected, the MED is given approximately by the product of the IMFP and the cosine of the emission angle. The latter estimates of the MED can be sufficient for emission angles larger than 50° although better estimates can be obtained, e.g. from the database.[1] If the total film thickness is greater than three times the largest MED, XPS can be used under certain conditions (see Annex D) together with ion sputtering to determine the variation of chemical composition with depth.

Table 1 provides a summary of the XPS methods which can be used for determining chemical composition and/or film thickness. Some methods can be utilized for the characterization of single-layer or multiple-layer thin films on a substrate and some methods can be used to determine the composition-depth profile of a sample for which the composition is a function of depth measured from the surface (i.e. where there is not necessarily an interface between two or more phases). The choice of method typically depends on the type of sample and the analyst's knowledge of the likely or expected morphology of the sample (i.e. whether the sample can consist of a single overlayer film on a flat substrate, multiple films on a flat substrate, or a sample with composition varying continuously with depth), whether the total film thickness is less than or greater than the largest MED for the detected photoelectrons, and the desired information (i.e. film composition or film thickness). The first three methods in Table 1 are non-destructive while the final method is destructive (i.e. the composition of the exposed surface is determined by XPS as the sample is etched by ion bombardment). Brief descriptions of these methods are given in the following clauses and additional information is provided in the indicated annexes.

Table 1 — XPS methods for the characterization of thin films on substrates and for samples with composition varying with depth

Clause	Method	Sample morphology	Film thickness less than three times MED?	Information obtained	Additional information
5.2	General XPS	Single and multiple films on a flat substrate	Yes	Layer order, film thickness, and film composition	Annex A
5.3	Angle-resolved XPS	Multiple films on a flat substrate Sample with composition varying with depth	Yes	Film thickness and film composition Composition as a function of depth	Annex B
5.4	Peak-shape analysis	Multiple films on a flat substrate Sample with composition varying with depth	Yes	Film thickness and film composition Composition as a function of depth	Annex C
5.5	Variable photon energy XPS	Multiple films on a flat substrate Sample with composition varying with depth	No	Film thickness and film composition Composition as a function of depth	
5.6	XPS with sputter-depth profiling	Multiple films on a flat substrate Sample with composition varying with depth	No	Film thickness and film composition Composition as a function of depth	Annex D

XPS is typically performed with laboratory instruments that are often equipped with monochromated Al Kα or non-monochromated Al or Mg Kα X-ray sources. For some applications, XPS with X-rays from synchrotron-radiation sources is valuable because the energy of the X-ray exciting the sample can be varied. XPS with Ag X-rays is also used to observe deeper regions compared to excitation with Al X-rays. In some cases, X-ray energies less than the Mg or Al Kα X-ray energies can be selected to gain enhanced surface sensitivity while in other cases, higher energies are chosen to gain greater bulk sensitivity and to avoid artefacts associated with the use of sputter-depth profiling.

Analysts should be aware of possible artefacts in XPS analyses. These artefacts include sample degradation during X-ray irradiation, reactions of the sample with gases in the ambient vacuum, and many effects that can occur during sputtering-depth profiling.[3]

5.2 General XPS

For a uniform thin film on a flat substrate, the film thickness can be determined from a ratio of a photoelectron peak intensity of an element in the substrate for a particular emission angle when an overlayer film is present to the corresponding intensity when the film is absent. Alternatively, the thickness can be obtained from a ratio of photoelectron peak intensity for an element in the film to the corresponding intensity for a thick film (i.e. a film with a thickness much greater than three times the MED). The composition of the film can be determined by the RSF method. Additional information is in Annex A.

For multiple thin-film analysis, it is important to determine the relative order of the layers above the substrate. We can estimate the layer order, thicknesses, and compositions by measuring the changes of peak-intensity ratios of components at two widely separated emission angles. Further details are in Annex A.

5.3 Angle-resolved XPS

Angle-resolved XPS (ARXPS)[4] can be utilized to determine composition as a function of depth for depths up to three times the largest MED of the detected electrons. The composition can be found for each film of a multilayer film on a substrate or the distribution of composition with depth can be determined for samples with no phase boundaries. For the former type of sample, film thicknesses can be estimated. Further details are in Annex B.

5.4 Peak-shape analysis

Peak-shape analysis,[5] the analysis of a photoelectron peak and its associated region of inelastically scattered electrons, can be utilized to determine composition as a function of depth for depths up to three times the largest MED of the detected electrons. The analyst can know the expected morphology of the sample (i.e. the distribution of composition with depth) or can often deduce the likely morphology from peak-shape analysis. Further details are in Annex C.

5.5 Variable photon energy XPS

Variable photon energy XPS can be employed to determine composition as a function of depth for depths up to three times the largest MED of the detected electrons.[6] XPS measurements of this type are typically performed with synchrotron radiation over a sufficiently wide photon energy range to give a useful range of MEDs of the detected photoelectrons.

5.6 XPS with sputter-depth profiling

Since 1985, “small-spot” XPS systems have been developed with lateral resolutions of commercial instruments less than 10 µm. Ion guns with focused beams have also become available so that faster sputtering of smaller regions on a sample became possible. Recent materials developments (e.g. the development of new gate oxides for semiconductor devices and the development of many types of nanostructures) have stimulated the growing use of XPS with sputter-depth profiling. It has also become necessary to obtain composition-depth profiles for inorganic and organic thin films without causing significant damage. XPS with sputter-depth profiling of such materials has now become possible with the development of buckminsterfullerene (C_{60}), argon cluster, water cluster, and other cluster-

ion sources. Low damage and low contamination by residual carbon have been reported in XPS depth profiling of several polymers using an Ar cluster-ion beam[7] and a C_{60} ion beam.[8] [9] Further details are in Annex D.

6 Specimen handling

Various types of thin-film specimens of metals, semiconductors, inorganic compounds, and polymers can be analysed by XPS. Guidelines for the preparation and mounting of specimens for analysis are given in ISO 18116[10] and ISO 18117.[11]

7 Instrument and operating conditions

7.1 Instrument calibration

The following ISO procedures should be performed to calibrate or check the performance of the XPS instrument or the analyst should check the instrument's performance by following the manufacturer's instructions or equivalent documentation.

a) calibration and checks of the binding-energy scale with ISO 15472[12]

b) checks of the repeatability and constancy of the intensity scale with ISO 24237[13]

c) checks of the linearity of the intensity scale with ISO 21270[14]

7.2 Operating conditions

7.2.1 Energy resolution

The main purpose of a wide scan is qualitative analysis. A full width at half maximum (FWHM) for the Ag $3d_{5/2}$ photoelectron peak of 2 eV is recommended for a wide scan. Narrow-scan spectra will provide quantitative information and chemical-state information and an energy resolution of less than 1 eV FWHM for the Ag $3d_{5/2}$ peak is recommended.

7.2.2 Energy range and step size

The energy range for a wide-scan spectrum shall be large enough to include the C KLL Auger peak and other potentially valuable peaks for the planned XPS analysis. The energy range should be 1 200 eV for Mg Kα X-rays and 1 400 eV for Al Kα X-rays. A step size of 1,0 eV is adequate when the energy resolution for a wide scan described in 7.2.1 is about 2 eV. For narrow scans (i.e. for chemical state analysis, quantification, or other mathematical manipulations of the XPS data), the step size should be 0,05 eV or 0,1 eV.

7.2.3 Multiple scans

Multiple scans are recommended for the acquisition of both wide scans and narrow scans to allow checks to be made of any changes in the XPS spectrum with time (e.g. can occur due to changes in X-ray intensity or to sample damage under X-ray irradiation).

7.2.4 Charge control and charge correction

Surface charging is likely for insulating samples. Techniques for charge control and charge correction are described in ISO 19318.[15] It is often convenient to use a reference C 1s binding energy between 284,6 eV and 285 eV for an observed peak due to carbonaceous contamination.[16] It is often very difficult to control the surface potential of a rough surface.

8 Reporting XPS method, experimental conditions, analysis parameters, and analytical results

8.1 XPS method for thin-film analysis

The method chosen for XPS thin-film analysis (as summarized in Clause 5 and described in Annexes A, B, C, and D) shall be reported.

EXAMPLE 1 Angle-resolved XPS.

EXAMPLE 2 Peak-shape analysis.

EXAMPLE 3 XPS with sputter-depth profiling.

8.2 Experimental conditions

8.2.1 Introduction

The experimental conditions for the XPS measurements shall be reported. Values of the parameters described in 8.2 shall be reported. In addition, information on the XPS instrument and the experimental conditions described here shall be reported. Examples of experimental parameters and their descriptions are given in Table 2.

8.2.2 XPS instrument

The name and model of the instrument used for the XPS measurements shall be reported. If any components on the instrument are not standard for the particular model, information shall be provided on the manufacturer or on the relevant design characteristics.

EXAMPLE The instrument used for the XPS experiments was a PHI Quantera SXM.

8.2.3 XPS analyser

Analyser conditions including the electron energy analyser, the acceptance angle of the input lens, the analysed area on the sample from which signals are detected, the pass energy in eV, the energy resolution in eV, the measured binding energy ranges for each peak in eV, and the energy step in eV shall be reported.

EXAMPLE The acceptance angle of the analyser was ±20°, the acceptance area was 1 × 0,5 mm^2, the pass energy was 55 eV, the energy resolution for the XPS measurements with the X-ray source of 8.2.4 was 0,6 eV, the measured binding energy range for the Si 2p peak was 115 eV to 95 eV, and the energy step was 0,1 eV.

8.2.4 X-ray source

The type of X-ray source (e.g. Mg Kα, Al Kα, monochromatic Al Kα, use of other anodes in the X-ray source, or synchrotron radiation), the photon energy in eV, the irradiation area on the sample, and the power dissipated in the X-ray anode shall be reported. The X-ray spot size should be described together with its measurement method, if known.

EXAMPLE 1 Monochromatic Al Kα X-rays were used, the photon energy was 1 486,6 eV, the power in the X-ray anode was 50 W, and the irradiation area on the sample was 1,5 × 0,4 mm^2. The X-ray spot was circular with a diameter estimated using the knife-edge method of 100 µm. The spot diameter was measured from a line scan and corresponded to the distance between the points where the photoelectron intensity was 50 % of the difference in the intensities in the plateau regions away from each edge in the direction of the scan.

EXAMPLE 2 Conventional Mg Kα X-rays were used, the photon energy was 1 253,6 eV, and the irradiation area on the sample was approximately 10 × 20 mm^2 at 300 W.

8.2.5 XPS configuration

The XPS configuration including the angle between the X-ray direction on the sample and the average analyser acceptance direction, the angle of X-ray incidence on the sample with respect to the surface normal, the photoelectron emission angles with respect to the surface normal, and the analyser azimuth angle with respect to the plane of X-ray incidence shall be reported.

EXAMPLE The angle between the X-ray direction and the analyser axis was 45°, the X-rays were incident normally on the sample surface, the emission angles of the photoelectrons were 0°, 25°, 37°, 45°, 53°, and 58° with respect to the surface normal, and the analyser azimuth was 22,5° with respect to the plane of X-ray incidence.

8.2.6 Charge control

The particular instrumental component(s) used for charge control shall be reported. The particular experimental conditions for charge control (such as the beam voltage in V and the total beam current in μA for the electron beam from a flood gun) shall be reported.

EXAMPLE For the flood gun, the beam voltage was –1,4 V (with respect to instrumental ground) and the total beam current was 10 μA measured on clean silver.

8.2.7 Ion gun parameters for sputter-depth profiling

Ion gun parameters for sputter-depth profiling such as ion species, beam voltage, beam current, spot size, raster size, incidence angle, sputter rate, and mass filter (if used) shall be reported.

EXAMPLE 1 The ion species was Ar^+, the beam voltage was 1 kV, the beam current was 500 nA, the spot size was 300 μm, the raster size was 2 × 2 mm^2, the incidence angle was 45°, and the sputter rate for SiO_2 was 3 nm/min.

EXAMPLE 2 The ion species was C_{60}^+, the beam voltage was 10 kV, the beam current was 10 nA, the spot size was 100 μm, the raster size was 2 × 2 mm^2, the incidence angle was 20°, the sputter rate for SiO_2 was 3 nm/min, and a mass filter was used to choose a 10 keV C_{60} ion beam.

8.3 Analysis parameters

8.3.1 Introduction

All methods and parameters used in the data analysis shall be reported. Some methods and parameters such as the transmission-function correction for the analyser, the method used for peak-intensity calculation (such as peak area or peak height), and the method used for background subtraction (and the starting and ending energies) are common to all XPS methods described here. If film compositions are reported, the type of relative sensitivity factor and the values of these factors shall be reported for each peak. Examples of analysis parameters and their descriptions are given in Table 3.

EXAMPLE The transmission-function correction was made from measurements of peak area/pass energy versus retarding ratio, peak areas were used for intensity calculations, the iterated Shirley background was used, the starting and ending binding energies for the Si 2p peak were 107 eV and 97 eV, respectively, and the average matrix relative sensitivity factors for the Si 2p was 0,368.

8.3.2 IMFP

Values of the IMFPs used in film-thickness calculations by general XPS, peak-shape analysis, and XPS with sputter-depth profiling shall be reported together with the source of the data.

EXAMPLE The IMFP for the Si 2p peak with Al Kα X-rays of 3,2 nm was obtained from the TPP-2M equation.[17]

8.3.3 Single-scattering albedo

Values of the single-scattering albedo, if used in film-thickness calculations as described in Annex A, should be reported.

EXAMPLE The single-scattering albedo for the Si 2p peak with Al Kα X-rays was 0,111. This value was calculated from the ratio of the IMFP to the sum of the IMFP and TRMFP,[18] as described in Annex A.

8.3.4 Parameters for peak-shape analysis

The chosen structure model (e.g. buried thin film, exponential depth profile, homogeneous depth profile, substrate with overlayer) and values of the parameters B, C, and D in the selected Tougaard inelastic-scattering cross-section formula (e.g. for metals and oxides, polymers, SiO_2, Si, Ge, and Al[83]) shall be reported. Information on the structure models and the various parameters is given in Annex C.

EXAMPLE A substrate with an overlayer was the chosen morphology model and recommended values of the parameters B and C for metals and oxides of 2 866 eV^2 and 1 643 eV^2, respectively, were used (the parameter D was not used).

8.3.5 Parameters for angle-resolved XPS

The type of algorithm used for depth profile reconstruction shall be reported. If the maximum entropy algorithm is used, the value of the regularizing constant for the final results shall be reported. Any corrections applied in the calculation of the depth profiles (e.g. for the asymmetry parameter, sample crystallinity, surface roughness, and elastic scattering) shall be reported. Information on analysis algorithms and corrections is given in Annex B.

EXAMPLE The maximum entropy method was used. The value of the regularizing constant α was fixed at 5×10^{-4} during the calculation.[19]

8.3.6 Special methods

Any special methods used for data analysis (e.g. curve fits to extract chemical states, linear least-square fitting, target factor analysis) shall be reported.

EXAMPLE A curve fit was applied to the Si 2p spectrum to determine the intensities of the metal and oxide chemical states.

8.4 Examples of summary tables

Summary tables for methods, acquisition parameters, and analysis parameters, as shown in Tables 2 and 3, can be convenient and useful for day-to-day use.

Table 2 — Examples of experimental conditions to be reported, as described in 8.2

Parameters	Description
Date	2010–04–01
Sample description	SiO_2(2,0 nm)/Si(100) (substrate)
XPS method	Film thickness analysis Peak-shape analysis
XPS instrument	PHI Quantera SXM
XPS configuration	
Angle between analyser and X-ray source	45°
Emission angle	45°
Analyser azimuth	22,5° with respect to the plane of X-ray incidence
Analyser condition	

Table 2 *(continued)*

Parameters	Description
Type of electron energy analyser	Concentric hemispherical analyser (CHA)
Acceptance angle	±20°
Acceptance area	1 × 0,5 mm^2
Photoelectron peak 1	Si 2p
Energy range	112 ~ 92 eV
Energy step	0,1 eV
Pass energy	55,0 eV
Photoelectron peak 2	O 1 s
Energy range	542 ~ 522 eV
Energy step	0,1 eV
Pass energy	55,0 eV
Photoelectron peak 1	C 1s
Energy range	298 ~ 278 eV
Energy step	0,1 eV
Pass energy	55,0 eV
X-ray source condition	
Type of X-ray source, energy, and power	Monochromatized Al Kα, 1 486,6 eV, 25 W
Expected spot size	100 µm in diameter
Charge control	1,4 eV 10 µA electron and 7 eV 35 nA Ar ion beam irradiation
Sputter on beam	Not used for this analysis but typical value for sputter cleaning is described below
Gas species	Ar
Beam voltage and current	1 kV, 500 nA
Spot size	300 µm in diameter
Raster size	2 × 2 mm^2
Incident angle	40°
Sputter rate for SiO_2	3 nm/min
Mass filter	None

Table 3 — Examples of analysis parameters to be reported, as described in 8.3

Parameters	Description
Analysis mode	Film thickness
General parameter	The transmission-function correction was made from measurements of peak area/pass energy versus retarding ratio, peak areas were used for intensity calculations, the iterated Shirley background was used, the starting and ending binding energies for the Si 2p peak were 107 eV and 97 eV, respectively, and the average matrix relative sensitivity factors for the Si 2p peak was 0,368
Inelastic mean free path	3,2 nm for Si 2p peak with Al Kα X-rays
Single-scattering albedo	ω = 0,111 for Si 2p peak with Al Kα X-rays
Parameters for peak-shape analysis	Not applicable
Parameters for angle-resolved XPS	Not applicable
Special method	Curve fit to extract elemental Si and Si oxide peaks

8.5 Analytical Results

Depending on the detail requested by a customer, the following analytical results shall be reported together with the chosen analysis method (as listed in Table 1).

a) film layer order

b) film thickness and composition

c) composition as a function of depth

The recording and reporting of these information should follow ISO 16243.[20]

Details and examples of the XPS analysis methods described are shown in Annexes A, B, C, and D. Table 1 can be used to select an analysis method that is suitable for the desired information.

Annex A
(informative)

General XPS

A.1 Introduction

Methods to obtain thin-film thickness, thin-film composition, and the structure of a multilayer film are described. In structure analysis, the relative order of the layers above the substrate or the relative depths of different functional groups can be obtained.

A.2 Symbols and abbreviated terms

AMRSF Average matrix relative sensitivity factor

ARSF Atomic relative sensitivity factor

EAL Effective attenuation length

E_f Energy of the photoelectron emitted from the overlayer

E_S Energy of the photoelectron emitted from the substrate

ERSF Elemental relative sensitivity factor

$I_A^{\theta_L}$ Intensity of component "A" at lower emission angle

$I_A^{\theta_H}$ Intensity of component "A" at higher emission angle

$I_B^{\theta_L}$ Intensity of component "B" at lower emission angle

$I_B^{\theta_H}$ Intensity of component "B" at higher emission angle

I_f Intensity of photoelectrons emitted from the overlayer ("overlayer signal")

I_n Intensity of photoelectrons emitted from *n*th layer from the top

I_{n+1} Intensity of photoelectrons emitted from *n+1*th layer from the top

I_S Intensity of photoelectrons emitted from the substrate and transmitted through the thin-film overlayers

I_0^f Intensity of photoelectrons emitted from the semi-infinite overlayer material

I_0^s Intensity of photoelectrons emitted from the semi-infinite substrate

L_n Effective attenuation length of the photoelectron in the *n*th layer

L_{n+1} Effective attenuation length of the photoelectron in the *n+1*th layer

$L(E)$ Effective attenuation length at kinetic energy E

N_0	Atomic density of the oxide overlayer
N_e	Atomic density of the substrate
Q_o	Elastic-scattering correction factor in the overlayer
Q_e	Elastic-scattering correction factor in the substrate
$R_{A/B}$	Ratio of intensities at high emission angles of component A to B and low emission angles of component A to B
R_{expt}	Ratio of intensities for photoelectrons emitted from the oxide-overlayer and the substrate
RSF	Relative sensitivity factor
R_o	Ratio of intensities of photoelectrons emitted from the bulk oxide and the bulk substrate material
s_n	Relative sensitivity factor of the component in the *n*th layer
s_{n+1}	Relative sensitivity factor of the component in the *n+*1th layer
t	Thickness of the thin-film overlayer
t_n	Thickness of the *n*th layer
t_{n+1}	Thickness of the *n+1*th layer
$W(\beta,\gamma)$	Angular distribution of photoemission from an atom as a function of β and γ
W_o	Angular distribution of photoelectrons emitted from the overlayer
W_e	Angular distribution of photoelectrons emitted from the substrate
x_e	Atomic fraction of the target element of the substrate
x_0	Atomic fraction of the target element of the overlayer
x_i	Atomic fraction of the element *i*
Z	Atomic number of an element
Z_{av}	Average atomic number
α	Angle of photoelectron emission with respect to the surface normal of the sample
β_{eff}	Effective asymmetry parameter, accounting for effects of elastic scattering on the photoelectron angular distribution in a solid
Γ	Angle between the direction of X-rays and the mean direction towards the analyser
Γ_i	Calculated, averaged, and interpolated coefficients for determining ζ
ζ	Ratio of the transport mean free path to the inelastic mean free path
λ_i	Inelastic mean free path
λ_e	Inelastic mean free path in the bulk substrate
λ_0	Inelastic mean free path in the bulk overlayer
λ_{tr}	Transport mean free path
ω	Single-scattering albedo

A.3 Film thickness analysis

The thickness of overlayer thin films can be measured by XPS when the overlayer film is homogeneous and uniform.

When the film thickness is less than about three times the MED for the target photoelectron peak and $\alpha \leq 58°$,[21] the overlayer film thickness t can be determined from Formula (A.1).

$$t = L\left(E_s\right)\cos\alpha \ln\left(\frac{I_s}{I_0^s}\right) \tag{A.1}$$

or

$$t = L\left(E_f\right)\cos\alpha \ln\left(1 - \frac{I_f}{I_0^f}\right) \tag{A.2}$$

where

α is the angle of photoelectron emission (with respect to the surface normal);

$L(E_S)$ and $L(E_f)$ are effective attenuation lengths (EALs) in the overlayer film at the substrate photoelectron energy E_S and the overlayer film energy E_f, respectively;

I_s and $I_0{}^s$ are photoelectron intensities measured from the substrate with the overlayer film and the bare substrate, respectively;

I_f and $I_0{}^f$ are measured intensities from the film and a thick layer of that film, respectively.

For peak intensity measurements, ISO 20903[22] should be utilized.

The EAL can be estimated from Formula (A.3)[2] when α ≤ 50° or from Formula (A.4) when α ≤ 58°[21]

$$L(E) = \lambda_i(1 - 0{,}735\omega) \tag{A.3}$$

or

$$L(E) = 0{,}979\,\lambda_i\,[\,1 - \omega\,(0{,}955 - 0{,}077\,\ln Z)] \tag{A.4}$$

where

$$\omega = \frac{\lambda_i}{\lambda_i + \lambda_{tr}} = \frac{1}{1+\zeta} \tag{A.5}$$

The value of ζ for element *i* can be estimated from Formula (A.6).[18]

$$\zeta_i = \exp[\Gamma_{i,3}\ln^3 E_i + \Gamma_{i,2}\ln^2 E_i + \Gamma_{i,1}\ln E_i + \Gamma_{i,0}] \tag{A.6}$$

where the values of $\Gamma_{i,3}$, $\Gamma_{i,2}$, $\Gamma_{i,1}$, and $\Gamma_{i,0}$ for element *i* can be obtained from a table in Reference [32]. For compounds or alloys, the Γ_m values for a material *m* can be estimated from the average atomic number Z_{av} for that material.

$$Z_{av} = \sum x_i Z_i \tag{A.7}$$

Values of Γ_m for Z_{av} can then be selected from the table in Reference [32]. If Z_{av} is not an integer, one can interpolate using Γ_m values for neighbouring elements.[18]

Values of λ_i can be obtained from the predictive TPP-2M equation [17][32] and a database.[23] Values of λ_{tr} can be obtained from two databases,[24][25] the computer code ELSEPA,[26] and a predictive equation.[27]

For a metal substrate with its oxide as an overlayer, the film thickness can be calculated using Formula (A.8).[28]

$$t = L(E)\cos\alpha\left(1 + \frac{R_{expt}}{R_o}\right) \tag{A.8}$$

where

R_{expt} is the ratio of photoelectron intensities from the oxide overlayer and the elemental substrate;

R_o is the corresponding ratio for the bulk solids (or sufficiently thick films).

It is recommended that R_o be measured experimentally using the same peak-fitting algorithm as that used for the analysis of the spectrum for the oxide sample to obtain an accurate measurement of the film thickness.[19] The value R_0 can also be calculated from References [21], [29], and [30].

$$R_o = \frac{x_o N_o Q_o(\alpha,\omega) W_o \lambda_o}{x_e N_e Q_e(\alpha,\omega) W_e \lambda_e} \tag{A.9}$$

$$W(\beta_{eff},\gamma)=\frac{1}{4\pi}\left\{1-\left[\beta_{eff}\left(3\cos^2\gamma-1\right)/4\right]\right\} \quad \text{(A.10)}$$

where

N_o is the atomic density in the oxide;

$Q_o(\alpha,\omega)$ is the elastic-scattering correction factor in the oxide;

W_o is the angular distribution of photoelectrons from the oxide;

λ_o is the inelastic mean free path in the oxide;

N_e, $Q_e(\alpha,\omega)$, W_e, and λ_e are the corresponding quantities in the substrate.

Guidelines for background subtraction from the obtained spectra are given in ISO/TR 18392[31] and ISO 20903.[22]

A.4 Chemical composition

RSFs are commonly used for quantification of unknown samples. The use of AMRSFs is recommended for photoelectron energies larger than 200 eV.[32] Guidelines for the quantitative surface analysis by XPS are given in ISO 18118.[32]

NOTE The use of RSFs is only recommended when the thin film is homogeneous and its surface is flat.

A.5 Structure analysis

In practical thin-film analysis, it is important to determine the relative order of the layers above the substrate or the relative position (depth) of different functional groups such as C = O, NO_2 within a particular layer. Seah et al. proposed a simple method to estimate the layer order by measuring the change of peak-intensity ratios of components at two-emission-angles (that were recommended to be 0° and more than 70° relative to the sample normal).[33] This method is called structure analysis and is utilized to determine the relative depths (from the surface) of layers in the sample. The larger the ratio of the photoelectron signal at the high emission angle to the low emission angle, the closer is the layer to the surface. Figure A.1 shows an example of spectra measured at low and high emission angles and Table A.1 shows the layer order established from the intensity ratios.

The same approach can also be used to estimate layer thicknesses and compositions. We designate the intensities of component "A" at lower and higher emission angles as $I_A^{\theta_L}$ and $I_A^{\theta_H}$, respectively. Similarly, the intensities of component "B" at lower and higher emission angles are $I_B^{\theta_L}$ and $I_B^{\theta_H}$, respectively. The ratio is then calculated as:

$$R_{A/B}=\frac{I_A^{\theta_H}}{I_A^{\theta_L}}\times\frac{I_B^{\theta_L}}{I_B^{\theta_H}} \quad \text{(A.11)}$$

If $R_{A/B}$ is larger than 1, component "A" is located above component "B" if the EALs of each component are almost the same. The relative depths of all components can be estimated by this procedure. If $R_{A/B}$ is close to 1, these components would be in the same layer. If $R_{A/B}$ is smaller than 1, component "A" is located under component "B".

After determination of layer order, iterated calculations can be performed for the intensity ratios using Formula (A12) to minimize the differences between calculated and measured intensities by changing the compositions and thicknesses of each layer.[34]

$$\frac{I_n}{I_{n+1}} = \frac{s_n t_n L_{n+1}}{s_{n+1} t_{n+1} L_n} \times \exp\left[\frac{1}{\cos\alpha}\left(\frac{t_n + \cdots + t_1}{L_{n+1}} - \frac{t_{n-1} + \cdots + t_1}{L_n}\right)\right] \tag{A.12}$$

The ratio of EALs in Formula (A.12) can be estimated from Formula (A.13).[35]

$$\left(\frac{L_{n+1}}{L_n}\right) = \left(\frac{E_{n+1}}{E_n}\right)^{0,75} \tag{A.13}$$

Formula (A.13) neglects any change in the atomic relative sensitivity factors for particular elements due to changes of chemical state. This method can be applied to thin films with a thickness that is less than a few times the EAL of the photoelectrons.

A.5.1 An example of structure analysis by the two-emission-angles method

Figure A.1 shows XPS spectra for a specimen consisting of a thin film with a high dielectric constant on a silicon substrate that were measured at two different emission angles.[36] From these spectra, the peak intensity ratios of the detected elements are obtained as shown in Table A.1. Using Formulae (A.11), (A.12), and (A.13), the structure as shown in Figure A.2 is obtained.

NOTE The two-emission-angles method is based on the assumption that each layer is composed of a single element, compound, or mixture. A detected element, however, could be distributed in more than one layer. If the layer composition is known from prior information, iterated calculations are required to obtain the film thickness by minimizing the differences between intensities calculated from Formula (A.12) and measured intensities by changing the compositions and thicknesses of each layer.

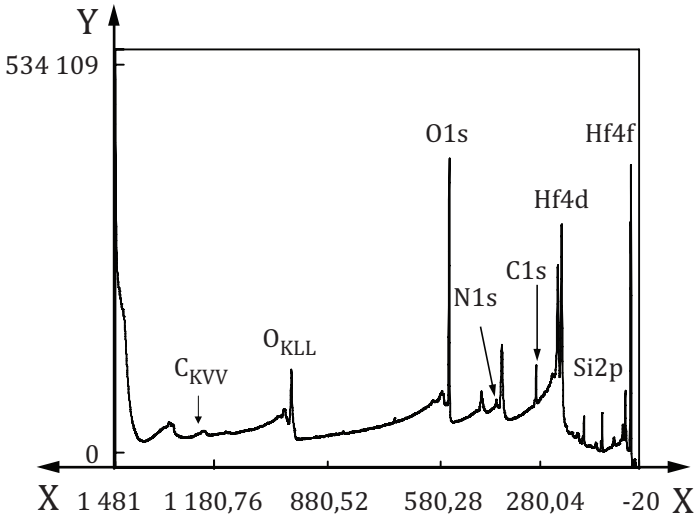

a) 0° from the surface normal

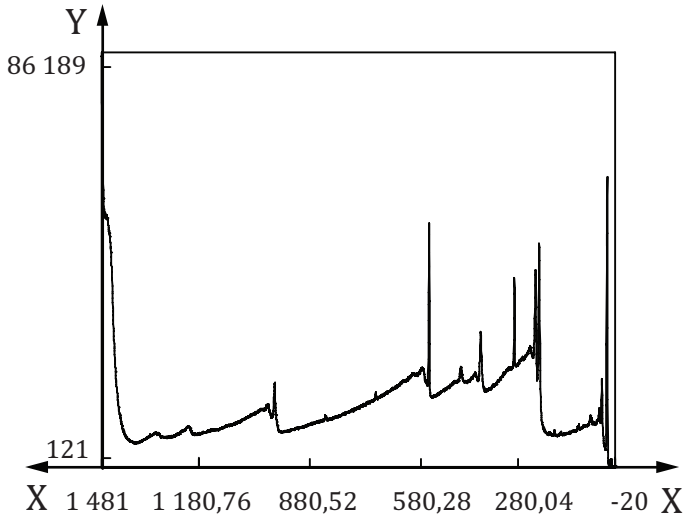

b) 73° from the surface normal

Figure A.1 — XPS spectra of a thin-film specimen measured at emission angles

NOTE The photoelectron peaks for O, N, C, Hf, and Si are detected.[36]

Table A.1 — Intensity ratios of photoelectron peaks at two-emission-angles (from the XPS spectra in Figure A.1)

Photoelectron peak	Intensity at angle 0°	Intensity at angle 73°	Intensity ratio I_{73}/I_0	Layer order
Hf 4f	1 051 384	166 280	0,158	2
Si 2p (substrate)	54 066	1 023	0,019	6
Si 2p (compound)	11 892	526	0,044	5
C 1s	97 096	37 746	0,389	1
N 1s	53 468	6 279	0,117	4
O 1s	701 805	95 218	0,136	3

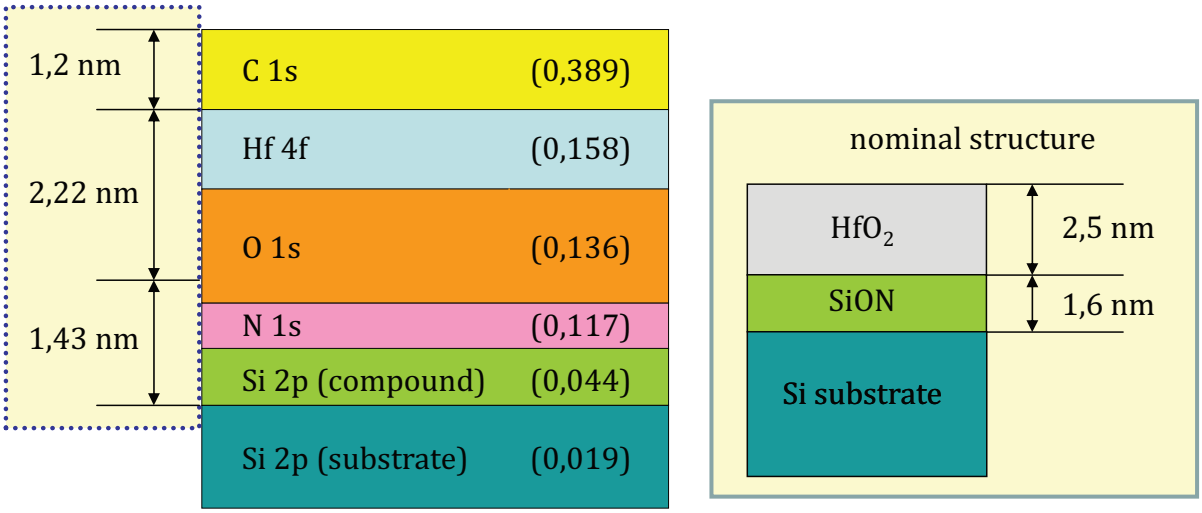

NOTE 1 The layer structure for the thin-film specimen used to obtain the XPS spectra in Figure A.1 is show on the left. The nominal structure of the specimen is shown on the right.

NOTE 2 The numerical values in parentheses are the ratios of measured peak intensities at an emission angle of 73° to those for normal emission.[36]

Figure A.2 — Layer structure for thin-film specimen used to obtain XPS spectra in Figure A.1

Annex B
(informative)

Angle-resolved XPS

B.1 Introduction

A description is given of algorithms for determining the in-depth distribution of the detected elements in XPS spectra acquired at multiple emission angles.

B.2 Symbols and abbreviated terms

A	Instrument transmission function
$c(z)$	Concentration of the element at depth z
$c_{j,k}^{calc}$	Calculated values of the atomic concentration of element j at angle k
$c_{j,k}^{obs}$	Observed values of the atomic concentration of element j at angle k
EAL	Effective attenuation length
$I_i(\theta)$	Photoelectron intensity of element i detected at angle θ from the surface normal
$I_j(\theta)$	Photoelectron intensity of element j detected at angle θ from the surface normal
L	Effective attenuation length
MED	Mean escape depth
MEM	Maximum entropy method
$m_{j,i}$	Initial atomic concentration of element j in ith layer
$n_{j,i}$	Simulated atomic concentration of element j in ith layer
Q	Joint probability function (maximum entropy method)
S	Entropy
S_i	Relative sensitivity factor of element i
S_j	Relative sensitivity factor of element j
T	Instrument transmission function
$W(\gamma)$	Angular distribution of photoelectrons emitted from a given atomic subshell (Asymmetry factor)
$X_i(\theta)$	Concentration of element i at emission angle θ
α	Regularizing constant that controls the extent of contribution of the entropy term
β	Asymmetry parameter for a given photoelectron peak assuming dipole transition
γ	Angle between the direction of incident X-rays and the analysed photoelectrons
θ	Angle of photoelectron emission relative to the surface normal of the sample

σ Photoionization cross section

$\sigma_{j,k}^2$ Unbiased variance of element j at angle k

χ^2 Chi-squared (statistics)

B.3 ARXPS measurement

ARXPS is performed by tilting the sample or by a parallel acquisition method. For the former method where only the sample is tilted and the angle between the X-ray source and the analyser is constant, anisotropy of photoemission is insignificant only if the angle between the X-ray source and the analyser is the 'magic' angle $\gamma \sim 54{,}7°$.

Algorithms for determining the in-depth distribution of an element are reported in References [4], [37], [38], [39], [40], and [41]. In recent years, the parallel acquisition method has been developed for rapid ARXPS analysis in many fields. The parallel acquisition method acquires spectra for a number of different emission angles simultaneously by utilizing a special lens-analyser system.

For obtaining a concentration depth profile from an ARXPS measurement, photoelectron intensities for at least two different emission angles are measured as the first step. The photoelectron intensities acquired as a function of emission angle are converted to the concentration of each component as a function of depth with a model calculation.

The photoelectron intensity F for a given orbital of a given element, under the assumptions listed below, can be written as:[42]

$$F(\theta) = TA\sigma W(\gamma) \int_0^\infty c(z) \exp\left(\frac{-z}{L\cos\theta}\right) dz \tag{B.1}$$

The assumptions made for Formula (B.1) are:[42]

a) The specimen is amorphous or finely polycrystalline within the analysis volume and photoelectron diffraction effects are negligible.

b) Elastic scattering can be neglected.

c) Refraction of electrons on leaving the specimen surface is negligible.

d) The EAL of a photoelectron is independent of the composition of the material through which it passes.

e) The surface of the specimen is smooth on an atomic scale.

f) The acceptance angle of the electron analyser is very small and finite solid-angle effects can be neglected.

g) The specimen is uniform in the xy-plane.

h) The algorithm used to evaluate the peak intensities can cope with widely varying relative intensities of poorly resolved peaks and widely varying backgrounds without introducing systematic errors.

These assumptions cannot always be valid but they are necessary in published methods for concentration-depth profile reconstruction.

The factor [$TA\sigma W(\gamma)$] in Formula (B.1) contains instrumental terms that depend on the emission angle θ. It is convenient to introduce the reduced intensity, I, defined as:[42]

$$I(\theta) = \frac{F(\theta)}{TA\sigma W(\gamma)} \tag{B.2}$$

Formula (B.1) can then be expressed as

$$I(\theta) = \int_0^\infty c(z) \exp\left(\frac{-z}{L\cos\theta}\right) dz \tag{B.3}$$

NOTE Formula (B.3) is essentially a Laplace transform. Restoration of a concentration-depth profile from Formula (B.3) requires inversion of the Laplace transform, which represents a class of ill-posed mathematical problems. The matrix inversion required to solve the problem has no unique solution. Furthermore, the inversion is extremely sensitive to errors or noise in the experimental data. In order to overcome these problems, a large number of algorithms for the calculation of concentration-depth profiles have been developed. [37] [43] [44] [45] [46] [47] [48] [49] [50] [51]

The measured atomic concentration of element i at emission angle θ is expressed as Formula (B.4) when the thin film contains N elements.

$$X_i(\theta) = \frac{I_i(\theta)/S_i}{\sum_{j=1}^{N} I_j(\theta)/S_j} \tag{B.4}$$

An estimated angular profile can be simulated from Formula (B.3) by changing the elemental distribution of the initial depth profile and comparing it with the measured angular profile.

The linear least-squares method or the regularization method is generally applied to the simulation, but there can be problems, e.g. the intensity of the data is limited and the uncertainty of the signal is assumed to be the same for data at all angles. The MEM can be a more suitable tool for obtaining a self-consistent result from a limited data set.[52] [53]

Regularization methods based on the Tikhonov regularization method and the MEM are briefly described. One way of recovering a concentration-depth profile $c(z)$ from Formula (B.3) is to minimize the sum of the squared errors.

$$\varphi = \left\| \int_0^\infty c(z) \exp\left(\frac{-z}{L\cos\theta}\right) dz - I(\theta) \right\|^2 \tag{B.5}$$

However, because of the ill-posed nature of the inversion, small variations in the measured intensity I result in very different profiles. One of the regularization methods, the Tikhonov regularization method,[54] [55] adds an additional term to Formula (B.5), as in Formula (B.6), to regularize the solution.

$$\varphi = \left\| \int_0^\infty c(z) \exp\left(\frac{-z}{L\cos\theta}\right) dz - I(\theta) \right\|^2 + \alpha \left\| c(z) \right\|^2 \tag{B.6}$$

The constant α, an arbitrary parameter, is a smoothing parameter that controls the contribution of the additional term to the smoothness of the depth profile. It is important to develop a criterion to select an α value so that it is large enough to stabilize the solution yet small enough to maintain real features existing in the depth profile.[44]

The entropy is given as:[43] [56]

$$S = \sum_{j=1}^{N} \sum_{i=0}^{p} \left[n_{j,i} - m_{j,i} - n_{j,i} \log \left(\frac{n_{j,i}}{m_{j,i}} \right) \right] \tag{B.7}$$

The MEM solution can be obtained by maximizing the entropy S when the chi-squared X^2 expressed in Formula (B.8) is within the uncertainty of measured ARXPS data.

$$\chi^2 = \sum_{j=1}^{N} \sum_{k=1}^{Nth} \frac{\left(c_{j,k}^{calc} - c_{j,k}^{obs} \right)^2}{\sigma_{j,k}^2} \tag{B.8}$$

These conditions can be met simultaneously by maximizing the joint logarithmic probability function, Q, expressed as Formula (B.9):

$$Q = \alpha S - \frac{\chi^2}{2} \tag{B.9}$$

NOTE A large value of α will result in an oversmoothed solution which is not in good agreement with the data. A small value of α will lead to overfitting the data by attempting to reproduce the noise in the data.

The measured angular profile might change by only a small amount after a change in the depth profile of a thin film. As a result, calculated solutions at a local minimum are easily obtained. Therefore, the following issues should be considered for MEM optimizations.

a) Two or more initial estimates of the depth profiles can be compared.[45] Particularly, optimizations of the parameters using prior information about the films are extremely important.

b) Bayesian statistical analysis can be used to determine the overall scaling of the noise in the experimental data, thus avoiding the need to estimate the point at which to stop the calculation with the maximum entropy solution.[45]

c) Other methods, such as Rutherford Backscattering Spectroscopy, can be compared with the ARXPS results.[57] [58]

Some of the factors that can cause uncertainty in the measurement and analysis of the ARXPS data are described below.

NOTE Additional guidance on the development of strategies for the analysis of ARXPS data have been published.[59]

B.3.1 Asymmetry factor

The factor $W(\gamma)$ in Formula (B.1) is the asymmetry factor which describes the angular distribution of photoemission. When elastic scattering is negligible and the excitation source is a conventional X-ray tube (i.e. non-polarized X-rays), $W(\gamma)$ is given by

$$W(\gamma) = 1 + \frac{1}{2} \beta \left(\frac{3}{2} \sin^2 \gamma - 1 \right) \tag{B.10}$$

where

β is the asymmetry parameter, a constant for a given photoelectron peak and photon energy dependence.

When the ARXPS measurement is carried out by tilting the sample on an instrument with γ close to 54,7°, the asymmetry factor is constant for all emission angles for a given orbital. However, for an instrument

with parallel ARXPS acquisition capability, the factor $W(\gamma)$ can vary as the emission angle is changed. This means that the photoelectron intensity measured by using a parallel ARXPS instrument should be corrected for the anisotropy of photoemission before it is quantified.

B.3.2 Crystallinity

It is well known that photoelectrons emitted from monocrystalline specimens give strong diffraction peaks.[60 61] A large amount of research on the effect of the modulation of photoelectron intensity attributed to diffraction has indicated that the selection of the measurement geometry and the angular intervals are critical for the quantification of ARXPS data acquired from monocrystalline samples or samples with a small number of oriented grains contributing to the measured signal.[62] [63] In order to avoid introducing inaccuracy related to crystallinity in the quantification process, it is recommended to acquire ARXPS data by using a number of different measurement geometries (e.g. different angular intervals and different azimuthal angles).

B.3.3 Surface roughness

Most of the algorithms for concentration-depth profile reconstruction or for film-thickness calculations from ARXPS measurements assume that the sample to be analysed has an atomically flat surface and planar interfaces. However, on the scale of the information depth, the surface roughness of industrial samples is generally high. The effect of surface roughness on the photoelectron intensity has been studied for some different models and it has been pointed out that the surface roughness can complicate the quantification of ARXPS data.[64] [65] [66] [67] [68] [69] [70] [71] [72]

B.3.4 Elastic scattering

Elastic scattering of photoelectrons is generally ignored in concentration-depth profile reconstruction algorithms. However, neglect of this factor causes an error in attenuation-length estimation, particularly when the measurement is performed at emission angles larger than about 60°. When electrons travelling towards smaller emission angles are elastically scattered in the near-surface region, they can be elastically scattered to travel towards larger emission angles.[29] Thus, at large emission angles, the intensity of the photoelectron signal from the substrate becomes higher than expected. It has been suggested that errors related to this effect can be minimized by using emission angles $\theta \leq 60$.[29] [73] [74] Nevertheless, the effects of elastic scattering can still be significant in modifying the measured intensity distributions and introducing artefacts in composition-depth profiles deduced on the basis of negligible elastic scattering.[75]

B.4 Remarks on data treatment for angle-resolved XPS

Figure B.1 shows a comparison of results from analyses of a set of ARXPS data using four algorithms for determining depth profiles. The sample for this example consisted of aluminium oxide on aluminium and was contaminated with two oxidation states of a silicon species of unknown origin and depth distribution.[73] Each method gave an excellent fit to the measured intensities as a function of emission angle. However, there were large differences among the derived depth profiles. Regularization and MEM gave more useful results, but the results shall be interpreted carefully because they depend on assumptions about the form of the depth profile or the composition of the specimen. Strong prior knowledge of the likely form of the depth profile is expected to improve the depth resolution.[73] Users of these nonlinear analysis methods should take great care when selecting constraints on the depth profile from the reconstruction.

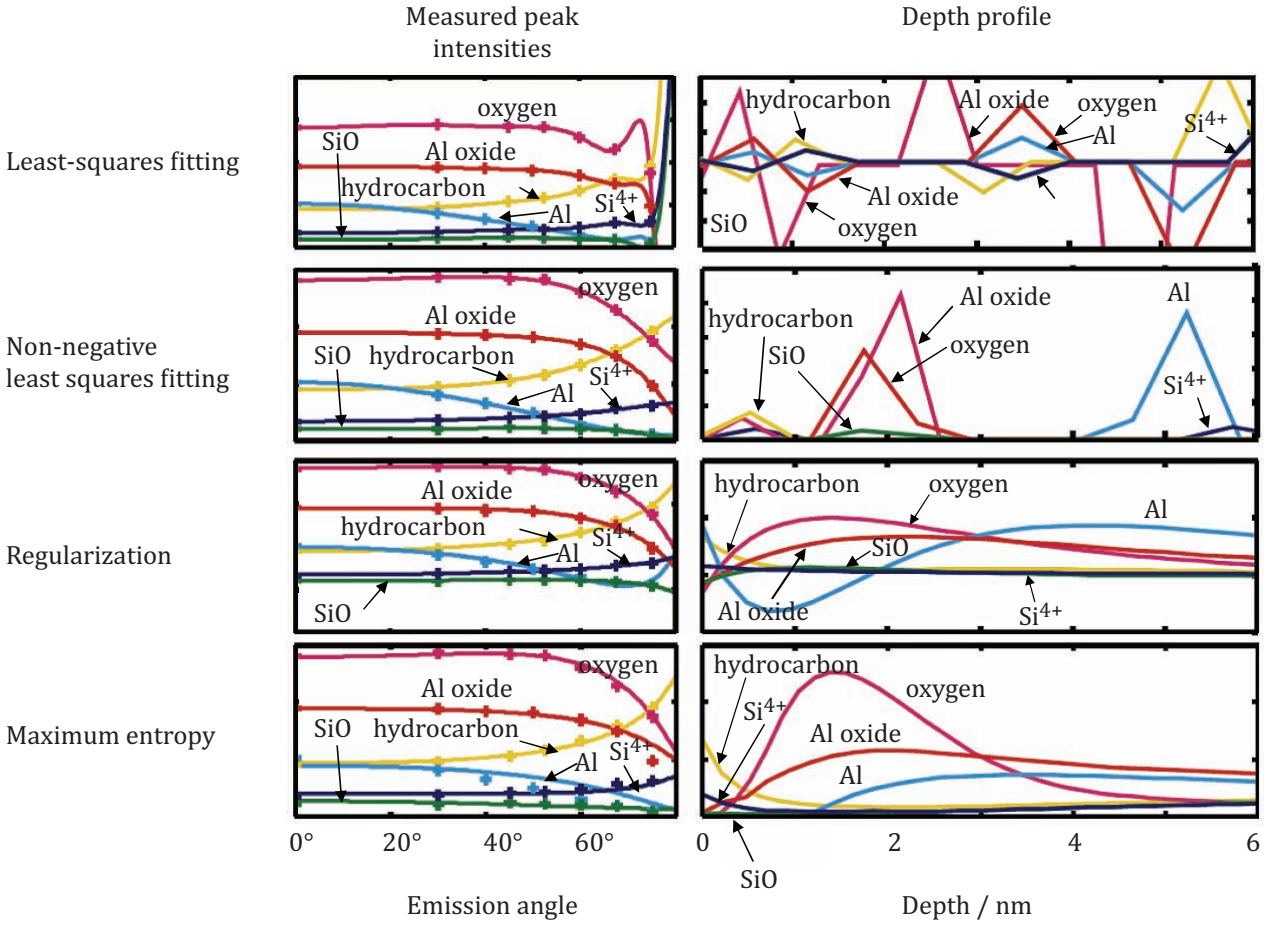

Figure B.1 — Comparison of four algorithms for recovering continuous depth profiles from ARXPS data[73]

Annex C
(informative)

Peak-shape analysis

C.1 Introduction

Peak-shape analysis of photoelectron spectra can give useful information on the near-surface morphology of a sample. A description is given here of peak-shape analysis for quantitative analyses of identified phases on a surface.

C.2 Symbols and abbreviated terms

AOS	Amount of substance in atoms/nm^2
A_p	Peak area
$A_p{}^H$	Peak area from a solid with a homogeneous atomic distribution of density c_H
c_H	Density in atoms/nm^3
d	Film thickness of a uniform film with the same atomic density as the reference material
dE_0	Energy interval at kinetic energy E_0
$F(E)$	True spectrum
$F(E_0,\Omega)$	True spectrum excited from an atom in an energy interval dE_0 at E_0 and solid angle Ω
$f(z)$	Atomic distribution as a function of depth
I_0	Intensity of photoelectrons emitted from the semi-infinite solid substrate
I_B	Background height
IMFP	Inelastic mean free path
$J(E)$	Measured XPS spectrum
$J(E,\Omega)$	Measured XPS spectrum
$K(T)$	Differential inelastic-scattering cross section
L	Decay length
s	Integration variable without physical significance
T	Energy loss in eV
z	Depth in nm
Ω	Solid angle
θ	Angle of photoelectron emission relative to the surface normal of the sample
λ	Inelastic mean free path in nm

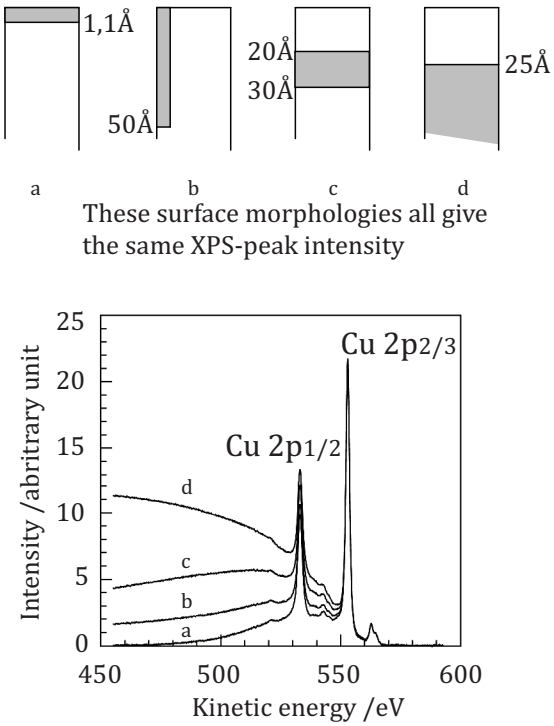

Figure C.1 — Four widely different surface and near-surface distributions of Cu atoms in and on Au that give identical Cu $2p_{3/2}$ peak intensities but quite different inelastic backgrounds[79]

C.3 Quantification strategy for peak-shape analysis

Since 1983, methods of varying degrees of complexity have been developed for extracting quantitative information from the large variations of the inelastic background associated with a photoelectron peak that depend on the depth distribution of the emitting atoms. All information is derived from an analysis of a single spectrum and is therefore also valid for rough surfaces when the photoelectron emission angle is close to the surface normal. The technique, developed by Tougaard et al.,[5] [76] [77] [78] [79] [80] [81] relies on the fact (see Figure C.1) that the inelastic background in the energy distribution of emitted electrons depends strongly and characteristically on the depth-concentration profile of the atoms responsible for the selected photoelectron peak.

Some electrons undergo inelastic-scattering processes on their way out of the sample and the typical energy loss in a single-scattering event is between 10 eV and 30 eV.[82] [83] Single and multiple inelastic scattering results in a fairly broad background with weak features corresponding to plasmon and interband transitions, but from a few solids (e.g. Al, Si, SiO_2,) clear plasmon peaks can be observed.[83] The multiple-scattering processes lead to a broad, measured energy distribution compared to the original distribution at the point of excitation in the solid.[76] [77] [78] The distance between inelastic-scattering events is only ~1 nm[17] [84] and the resultant *shape* of the background in a wide energy range, 50 eV to 100 eV below the characteristic photoelectron peaks, therefore, depends critically on the atomic depth distribution on the *nanometre* scale. This phenomenon can be used to enhance the accuracy of XPS quantification and to provide information on the depth distribution of the emitting atoms.[78] [79] [80] To interpret measured XPS spectra, it is useful to be able to intuitively identify information on the depth distribution from simple visual inspection of the shape of the background associated with the characteristic peaks.

Figure C.1 shows results of model calculations illustrating the dependence of the Cu 2p spectral shape on the depth distribution of copper atoms for four different distributions of Cu atoms on and in a gold matrix. The XPS Cu 2p peak intensity from all four solids is identical even though the Cu concentration

in the immediate surface varies between 0 % and 100 %, while the actual amount of Cu within the surface region can be anywhere between the equivalent of 0,11 nm (as in (a)) or 1,0 nm (as in (c)) or even greater (as in (d)). From this example, it is clear that peak areas can give only qualitative compositional information unless the atom depth distribution is known. For accurate quantification, the task of determining the atomic concentration, therefore, cannot be decoupled from the task of determining the depth distribution.

It is clear that the background contributions to the spectra over a wide energy range below the Cu peaks depend strongly on the depth distribution of the element. It is thus, experimentally, very easy to distinguish between the depth distributions contributing to the backgrounds of the four spectra in Figure C.1, over a 50 eV energy region.

Because the dependence of inelastic scattering on depth distribution is so strong, even quite simple and approximate models enhance the accuracy of quantification significantly and models with different levels of sophistication have been developed. These are described in the following subclauses. To make a clear description of the techniques, we will take a specific example, the spectrum in Figure C.2 from an iron sample that had been exposed to a maritime environment.

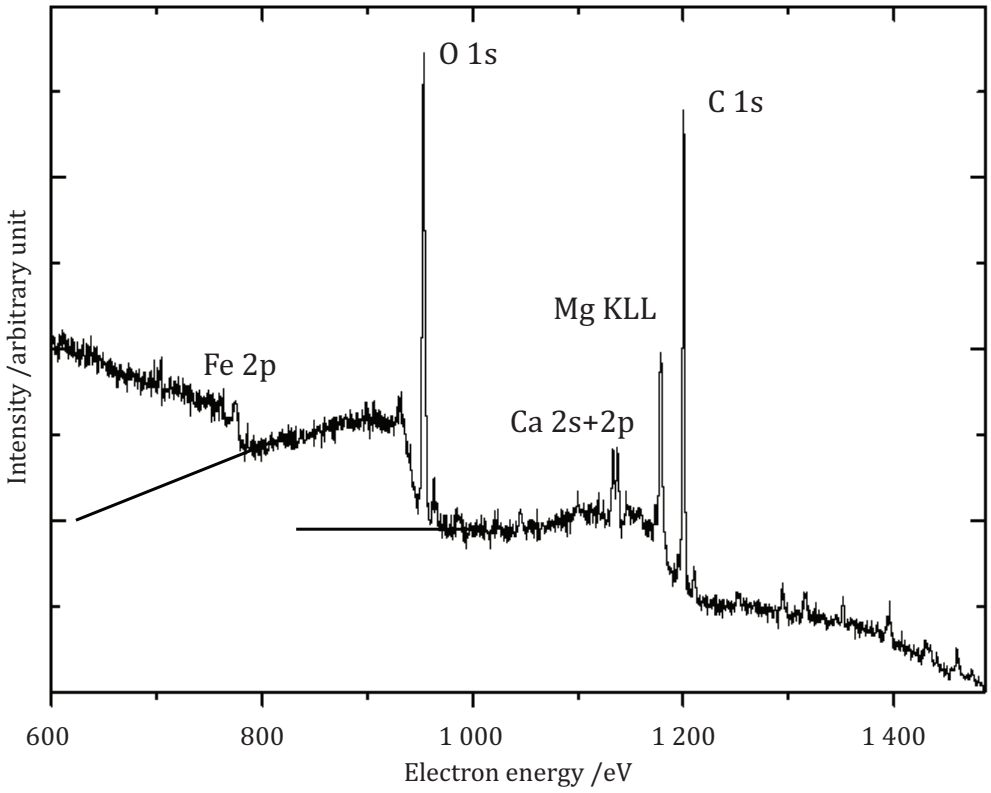

Figure C.2 — Al Kα-excited XPS spectrum from an Fe sample that had been exposed to a corrosive maritime environment, from Reference [85]

C.3.1 Visual inspection

Just by simple visual inspection of the Fe 2p spectrum in Figure C.2,[85] it is evident that the depth distribution is of type (d) in Figure C.1 rather than of any of the other types. It can thus be concluded that Fe was primarily in the bulk, while the O 1s background is of type (b) or (c), indicating that the oxygen atoms were confined mostly to the outermost atomic layers. It can be concluded immediately that, qualitatively, the sample consisted of an iron substrate covered with a fairly thick oxide layer. Thus, just a quick look at an XPS survey spectrum and comparing this to the classes of characteristic depth profiles and corresponding peak shapes in Figure C.1 can give a rough qualitative picture of the depth distributions of the various elements.

C.3.2 Peak area-to-background-intensity ratio A_p/I_B

The simplest quantitative description of the variation in peak shape and background with depth is to take the ratio of the peak area A_p to the increase in background height I_B at a chosen energy below the peak energy. This ratio is very sensitive to the in-depth distribution because A_p and I_B vary in opposite directions as a function of the depths of the atoms in a solid. For a homogeneous distribution of atoms, it has been shown that the ratio, $D_{0,}$ is almost constant (~23 eV), independent of material and peak energy. Deviations from this value can then be used to estimate the depth distribution of atoms.[76] [86]

The algorithm can be understood from Figure C.3. A_p is the peak area (of the Fe 2p doublet from Figure C.2) determined after a linear background has been subtracted (dashed line) from the measured spectrum (i.e. after a linear background had been subtracted from the Fe 2p region in Figure C.2). I_B is the increase in intensity measured 30 eV below the peak energy. (In the case of a doublet peak as in Figure C.3, the geometrical weighted centroid of the peak structure is used as the reference energy). A quick estimate of the in-depth distribution of atoms can then be found from the rules in Table C.1. For a given system, the method can be fine-tuned by calibrating D_0 against A_p/I_B determined from the analysis of a sample known to have a homogeneous atomic distribution with depth. An example of its application to the Fe spectrum in Figure C.2 is also shown in Figure C.3, which gives the value A_p/I_B = 3,9 eV. According to the rules in Table C.1, this result shows that Fe is deep in the bulk of the sample. For the O 1s peak, one gets A_p/I_B = 14,9 eV (see Table C.4) which, according to the rules in Table C.1, shows that the oxygen atoms are confined to shallower layers. Other examples of the practical application of this algorithm can be found in References [87] and [88].

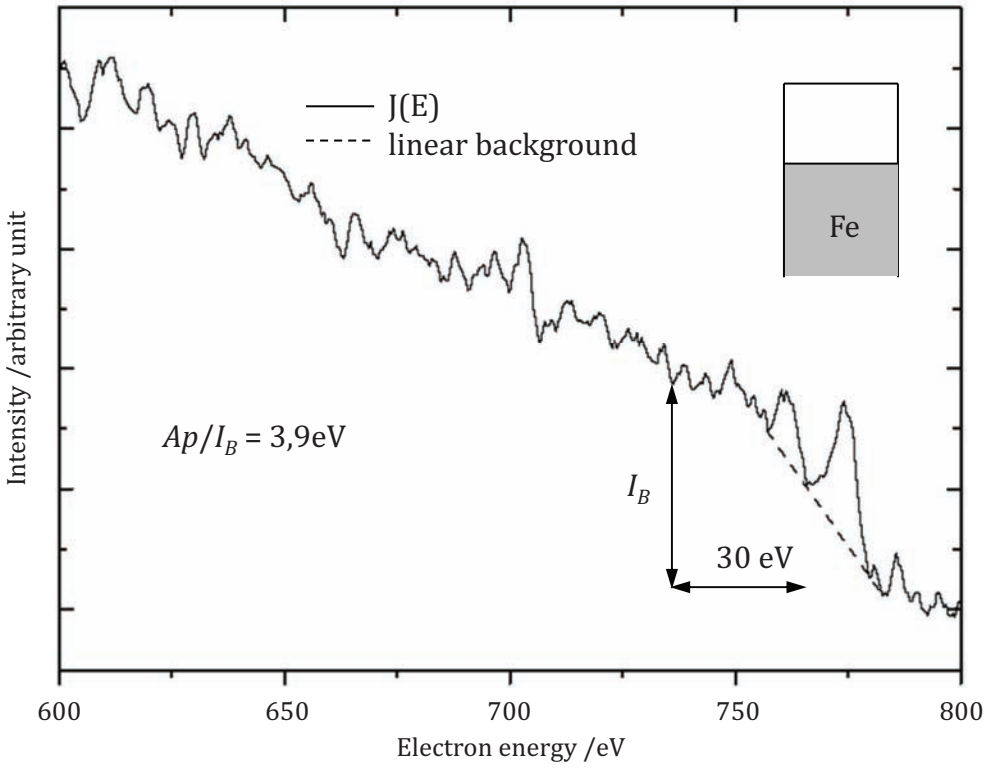

Figure C.3 — Example of the application of the A_p/I_B methods

Table C.1 — Rules for estimating the depth profile from A_p/I_B, from Reference [76]

A_p/I_B	Depth distribution
~23 eV	Uniform
>30 eV	Surface localized
<20 eV	Subsurface localized
If the same peak from two samples has the values $D_1 = (A_p/I_B)_1$ *and* $D_2 = (A_p/I_B)_2$ *then*	
if 30 eV < D_1 < D_2	atoms are surface localized in both samples and are at shallower depths in sample 2 than in sample 1
if D_1 < D_2 < 20 eV	atoms are primarily in the bulk of both samples and at deeper depths in sample 1 than in sample 2

C.3.3 Decay length *L* and amount of substance $(AOS)_{3\lambda}$

Another simple algorithm was first suggested in 1988-1990,[78] [9] [90] and later improved,[91] and its validity has been tested experimentally.[92] This algorithm provides quantitative information on the atomic depth distribution as well as on the amount of substance $(AOS)_{3\lambda}$, i.e. the number of atoms per unit surface area at depths z between 0 and 3λ. In this method, all depth distributions are approximated as exponential, i.e. $\exp(-z/L)$ where L is a characteristic decay length for the profile. The theoretical basis of the method is that the simple *Tougaard background*[92] is an exact solution in the analysis of the background for all depth profiles of exponential form and application of this to a general (not necessarily exponential) profile therefore determines the "best" exponential profile fit to the actual depth profile. If most atoms are at shallow depths, L will turn out to be small and positive, while if most atoms are at large depths, L will be small and negative. To be more specific, the method is as follows. The measured spectrum, $J(E)$, where E is the electron energy in *eV*, is first corrected by a standard *Tougaard background*, i.e.

$$F(E) = J(E) - B_1 \int_E^{E_{\max}} J(E') \frac{E' - E}{\left(C + (E' - E)^2\right)^2} \cdot dE' \tag{C.1}$$

where $C = 1\,643$ eV^2. For polymers and other materials (such as Si and Al) with sharp plasmon structures, the three-parameter Tougaard-background algorithm is more accurate, viz.

$$F(E) = J(E) - B_1 \int_E^{E_{\max}} J(E') \frac{E' - E}{\left(C + (E' - E)^2\right)^2 + D(E' - E)^2} \cdot dE' \tag{C.2}$$

where C and D depend on the material.[80] [83] The parameter B_1 is adjusted to give zero intensity ($F(E) = 0$) at a point 30 eV below the peak centroid (see the background dash-dotted line in Figure C.4) and from this, the decay length is determined.

$$L = \frac{B_1}{B_0 - B_1} \cdot \lambda \cdot \cos\theta \tag{C.3}$$

In Formula (C.4), B_0 is the value of B_1 determined from analysis, by Formula (C.1), of the spectrum from a homogeneous sample. In practice, B_0 is ~3 000 eV^2 for most materials.[80] The depth distribution is then estimated from the rules in Table C.2.[91] [92] A negative value of L corresponds to a depth distribution that increases with depth within the analysed depths (i.e. for z up to ~5λ). For a given system, the value B_0 can be fine-tuned by replacing B_0 by $B_1{}^H$ where $B_1{}^H$ is determined by 7analysis, from Formula (C.1), of a spectrum from a sample that is known to have a homogeneous atomic distribution.

Table C.2 — Rules for estimating the depth profile from *L*, from References [91] and [92]

L	Depth distribution
$6\lambda < \lvert L \rvert$	Almost uniform
$-3\lambda < L < 0$	Most atoms are at depths >1λ

Table C.2 *(continued)*

L	**Depth distribution**
$0 < L < 3\lambda$	Most atoms are at depths $<1\lambda$
If the same peak from two samples has values L_1 and L_2, then	
if $0 < L_1 < L_2$	atoms are surface localized in both samples and are at shallower depths in sample 1 than in sample 2
if $L_1 < L_2 < 0$	atoms are primarily in the bulk of both samples and at deeper depths in sample 2 than in sample 1

In Figure C.4, the decay-length method has been applied to the Fe 2p spectrum in Figure C.2 with the result that $L = -1{,}54\lambda$. From Table C.2, one can then conclude that the Fe atoms are at depths $> 1\lambda$. A similar analysis of the O 1s peak gives $L = -1{,}95\lambda$ (see Table C.4). This result shows that the O atoms are buried beneath the surface but are at shallower depths than Fe.

The *absolute* amount of substance within the outermost $\sim 3\lambda$ is[91]

$$(AOS)_{3\lambda} = \frac{L + \lambda \cdot \cos\theta}{1 - e^{-3\frac{\lambda\cos\theta + L}{L\cos\theta}}} \cdot A_p \frac{c_H}{A_p^H} \cdot \left(1 - e^{-3\lambda/L}\right) \tag{C.4}$$

where the peak area is

$$A_p = \int_{E_{p-30eV}}^{E_{\max}} F(E)\,dE \tag{C.5}$$

and A_p^H is the peak area from a solid with a homogeneous atomic distribution of density c_H. If the objective is to find the *relative* $(AOS)_{3\lambda}$ in a set of samples, it is not necessary to use a reference sample and determine c_H / A_p^H. It is often convenient to define an equivalent film thickness

$$d = \frac{AOS_{3\lambda}}{c_H} \tag{C.6}$$

which is the thickness of the material if it were distributed as a uniform film with the same atomic density as in the reference material. If c_H is in atoms/nm^3 and λ is in nm, then *AOS* is in atoms/nm^2 and d is in nm.

The validity of the algorithm in Formula (C.4) has been tested and found to give a good measure of the amount of substance, as well as a reliable depth sectioning based on both model and experimental spectra.[90] [91] [92] The accuracy of $(AOS)_{3\lambda}$ is typically better than ~15 % when this method is applied to a wide range of depth distributions. The algorithm is suitable for automation and can also therefore be applied to mapping where several thousand spectra at a time shall be analysed. The practical applicability of this algorithm for three-dimensional surface mapping has recently been demonstrated successfully.[93] It gives an image with much more quantitative information compared to the simple assumption that the concentration is proportional to the peak area (which is the standard method in XPS imaging), because in the latter case, the peak areas and hence the resulting maps, will not necessarily (see Figure C.1) reflect either the actual surface concentration or the amount of substance in the outermost atomic layers.

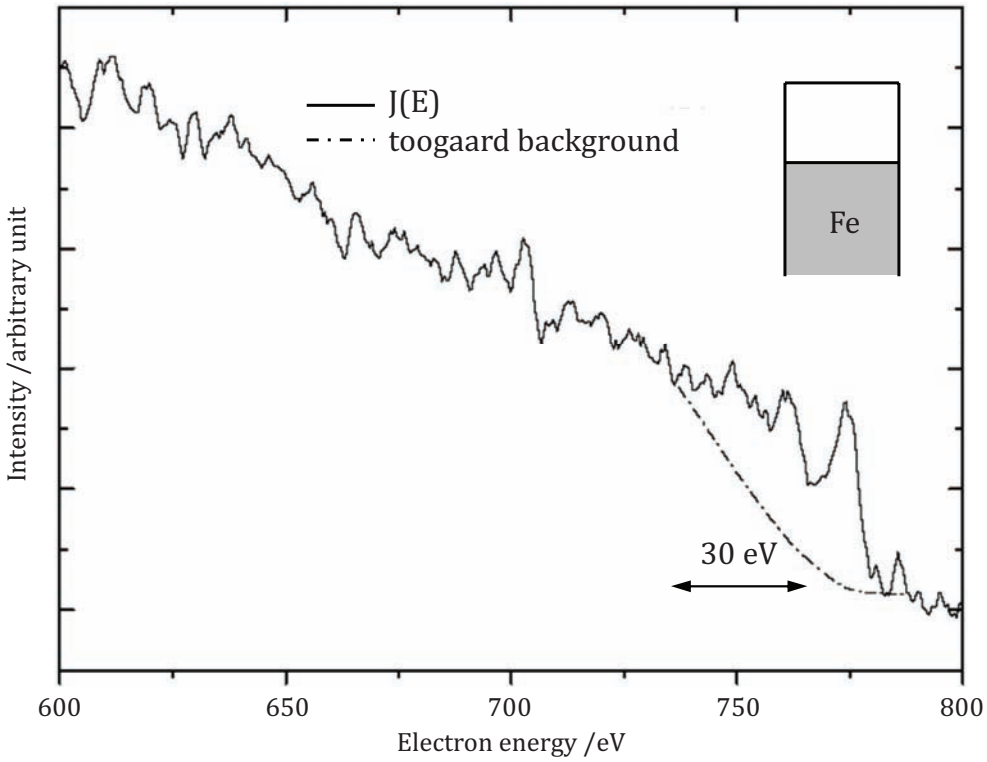

Figure C.4 — Example of the application of the decay length (*L*) methods

C.3.4 Quantification by detailed analysis of the peak shape

The above quantification procedures are easy to apply in practice. However, with greater effort and more elaborate algorithms, it is possible to obtain an even more accurate and detailed analysis of the near-surface elemental distribution. The underlying algorithms for this approach were published more than a decade ago and are summarized in Reference [79]. The validity of the technique has been established through a series of systematic experiments, some of which have been reviewed in Reference [80]. These studies have shown that quite detailed information on the in-depth atom distribution on the nanometre depth scale can be extracted. The algorithms are fairly complex but a user-friendly software package, which provides tools to do the full analysis from raw spectra to the resulting depth distribution, was developed to make this type of analysis available for non-specialists.[85] [94] The method is now widely used and has been applied to the study of a wide range of systems and physical phenomena, including thin-film growth mechanisms and subsurface elemental distributions of films, nucleation, island formation, diffusion, etching, etc.[95] [96] [97] [98] [99] [100] [101] [102] [103] [104] [105] Since the method is non-destructive, it also allows study of the changes in the surface morphology of a given surface atomic structure during surface treatment, as in chemical reaction or gradual annealing.

If elastic scattering, diffraction, and surface excitations are neglected, the measured XPS spectrum $J(E,\Omega)$ with atomic distribution $f(z)$ at depth z is[106] [107]

$$J(E,\Omega) = \int dE_0 F(E_0,\Omega) \int ds \exp\left[-i2\pi s(E-E_0)\right] \times \int dz f(z) \exp\left[-\frac{z}{\cos\theta}\sum(s)\right] \quad \text{(C.7)}$$

$$\sum(s) = \frac{1}{\lambda_i} - \int_0^\infty K(T)\exp(-isT)\,dT \tag{C.8}$$

where

f(z) is the number of atoms per unit volume at depth *z*;

$F(E_0,\Omega)$ is the true spectrum excited from an atom in an energy interval dE_0 at E_0 and solid angle Ω;

$K(T)$ is the differential inelastic-scattering cross section;

T is the energy loss (in eV);

s is an integration variable without physical significance.[108]

An algorithm for the removal of the inelastic background from measured spectra is effectively solved numerically by means of discrete Fourier transformation using a fast Fourier transformation algorithm.

The true initial excitation energy spectrum $F(E,\Omega)$ can be determined from analysis of the measured spectrum $J(E,\Omega)$.[79]

$$F(E,\Omega) = \frac{1}{P_1}\left\{J(E) - \frac{1}{2\pi}\int dE'J(E',\Omega)\int ds e^{-is(E-E')}\left(1-\frac{P_1}{P(s)}\right)\right\} \tag{C.9}$$

where

$$P(s) = \int f(z)\,e^{-\frac{z}{\cos\theta}\sum(s)}dz \tag{C.10}$$

with

$$P_1 = \int_0^\infty f(z)\,e^{-\frac{z}{\lambda\cos\theta}}dz \tag{C.11}$$

If information on $f(z)$ is known, $F(E,\Omega)$ can be determined.

For specific depth profiles, $f(z)$, part of the integrals in Formulae (C.10) and (C.11) can be done analytically. [109] [110] [65] [64] Table C.3 gives expressions for P_1 and $P(s)$ for different classes of depth profiles with parameters defined in Figure C.5.

As an example of the practical application of the method, the analysis of the XPS spectrum of the corroded iron sample in Figure C.2 will be described. Using the QUASES software,[85] the Fe 2p and O 1s energy regions are first isolated by subtracting straight lines fitted to the intensity on the high-energy sides of the peaks as shown in Figure C.2. The peaks isolated in this way are shown in Figure C.6. The spectra are then analysed with the QUASES software by varying the assumed depth profile and the corresponding background-subtracted spectra are calculated and plotted. In the upper panel of Figure C.6, Fe is assumed to be distributed homogeneously and it is clear that such a depth distribution does not account for the strong increase in background intensity. On the other hand, in the bottom panel, the assumption is that the Fe is distributed from a depth of about 3,5 nm to infinite depths and that is clearly a much better model for the peak shape and background over a wide energy region. The middle panel shows a similar analysis of the O 1s peak shape. The peak shape and background can be well described by assuming that the O atoms are distributed with constant concentration between depths of 2,5 nm and 8,0 nm. (The C 1s, Mg KLL, and Ca 2s and 2p peaks overlap somewhat in energy and an analysis of them would require a spectrum with a better signal-to-noise ratio. Furthermore, the separation of the peaks and simultaneous quantitative analysis can be done by the method in Reference

[110] which is also included in the software).[85] The conclusion from the analysis then is that the sample consists of an Fe substrate covered first with a layer of oxide about 5,5 nm thick, on top of which is a mainly carbonaceous layer of thickness about 2,5 nm. All this information was extracted from the rather noisy survey spectrum in Figure C.2.

Results from analyses of the peak shape for the XPS spectrum in Figure C.2 with the techniques described in C.3.1, C.3.2, C.3.3, and C.3.4 are compared in Table C.4. Note that the results from the simpler methods are in full agreement with the more detailed analysis in Figure C.6.

Table C.3 — Expressions for P_1 and $P(s)$ for different classes of depth profiles with the parameters defined in Figure C.5

Depth distribution function $f(z)$	P_1	$P(s)$
(Homogeneous and exponential depth profile as in Figure C.5 (a) $(C_s - C_b)\cdot e^{-z/L} + C_b$	$C_b\lambda_i\cos\theta + (C_s - C_b)\dfrac{L\lambda_i\cos\theta}{L+\lambda_i\cos\theta}$	$C_b\dfrac{\cos\theta}{\Sigma(s)} + (C_s - C_b)\dfrac{L\cos\theta}{L\cdot\Sigma(s)+\cos\theta}$
Delta layer profile $N\cdot\delta(z-z_0)$	$N\cdot e^{-\frac{z_0}{\lambda\cos\theta}}$	$N\cdot e^{-z_0\frac{\Sigma(s)}{\cos\theta}}$
Box-shaped profile for the atoms of type A as in Figure C.5 (b) $f_A(z) = \begin{cases} 0 \text{ for } 0<z<z_0 \\ C_A \text{ for } z_0<z<z_0+\Delta z \\ 0 \text{ for } z_0+\Delta z<z \end{cases}$	$C_A\cdot\lambda_i\cos\theta\cdot e^{-\frac{z_0}{\lambda_i\cos\theta}}\left[1-e^{-\frac{\Delta z}{\lambda\cos\theta}}\right]$	$C_A\dfrac{\cos\theta}{\Sigma(s)}$ $\times e^{-z_0\frac{\Sigma(s)}{\cos\theta}}\left[1-e^{-\Delta z\frac{\Sigma(s)}{\cos\theta}}\right]$
Box-shaped profile for the atoms of type B as in Figure C.5 (b) $f_B(z) = \begin{cases} C_B \text{ for } 0<z<z_0 \\ 0 \text{ for } z_0<z<z_0+\Delta z \\ C_B \text{ for } z_0+\Delta z<z \end{cases}$	$C_B\cdot\lambda_i\cos\theta$ $\times\left\{1-e^{-\frac{z_0}{\lambda_i\cos\theta}}\left[1-e^{-\frac{\Delta z}{\lambda_i\cos\theta}}\right]\right\}$	$C_B\dfrac{\cos\theta}{\Sigma(s)}$ $\times\left\{1-e^{-z_0\frac{\Sigma(s)}{\cos\theta}}\left[1-e^{-\Delta z\frac{\Sigma(s)}{\cos\theta}}\right]\right\}$
Island structures for the atoms of type A as in Figure C.5 (d), (e) and (f) $f_A(z) = \begin{cases} C_A \text{ for } 0<z<\Delta z_1 \\ f_1\cdot C_A \text{ for } \Delta z_1<z<\Delta z \\ 0 \text{ for } \Delta z<z \end{cases}$	$C_A\cdot\lambda_i\cos\theta$ $\times\left\{1-(1-f_1)\cdot e^{-\frac{\Delta z_1}{\lambda_i\cos\theta}} - f_1\cdot e^{-\frac{\Delta z}{\lambda_i\cos\theta}}\right\}$	$C_A\dfrac{\cos\theta}{\Sigma(s)}$ $\times\left\{1-(1-f_1)\cdot e^{-\Delta z_1\frac{\Sigma(s)}{\cos\theta}} - f_1\cdot e^{-\Delta z\frac{\Sigma(s)}{\cos\theta}}\right\}$
Island structures for the atoms of type A as in Figure C.5 (d), (e) and (f) $f_B(z) = \begin{cases} 0 \text{ for } 0<z<\Delta z_1 \\ (1-f_1)\cdot C_B \text{ for } \Delta z_1<z<\Delta z \\ C_B \text{ for } \Delta z<z \end{cases}$	$C_B\cdot\lambda\cos\theta$ $\times\left\{(1-f_1)\cdot e^{-\frac{\Delta z_1}{\lambda_i\cos\theta}} + f_1\cdot e^{-\frac{\Delta z}{\lambda_i\cos\theta}}\right\}$	$C_B\dfrac{\cos\theta}{\Sigma(s)}$ $\times\left\{(1-f_1)\cdot e^{-\Delta z_1\frac{\Sigma(s)}{\cos\theta}} + f_1\cdot e^{-\Delta z\frac{\Sigma(s)}{\cos\theta}}\right\}$

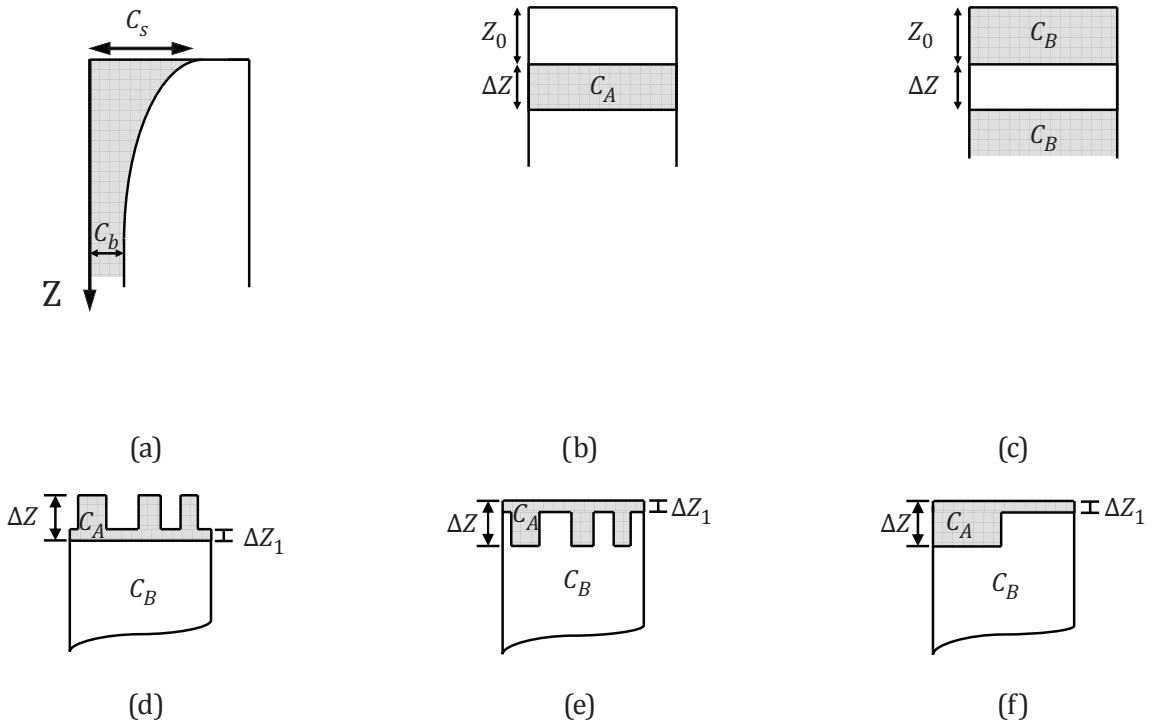

Figure C.5 — Definition of parameters for some in-depth profiles. The structures in (d), (e), and (f) give identical spectra

Table C.4 — Results from analysis of the O 1s and Fe 2p spectra in Figure C.6 and comparisons with results from the methods of C.3.1 (visual inspection), C.3.2 (A_p/I_B), and C.3.3 (decay length L)

Method of analysis	Fe	O
Visual inspection	subsurface	surface region
A_p/I_B	3,9 eV (subsurface localized)	14,8 eV (subsurface localized)
Decay length L	–1,54λ	–1,95λ
Detailed peak shape	3,5 - 100 nm	2,5 – 8,0 nm

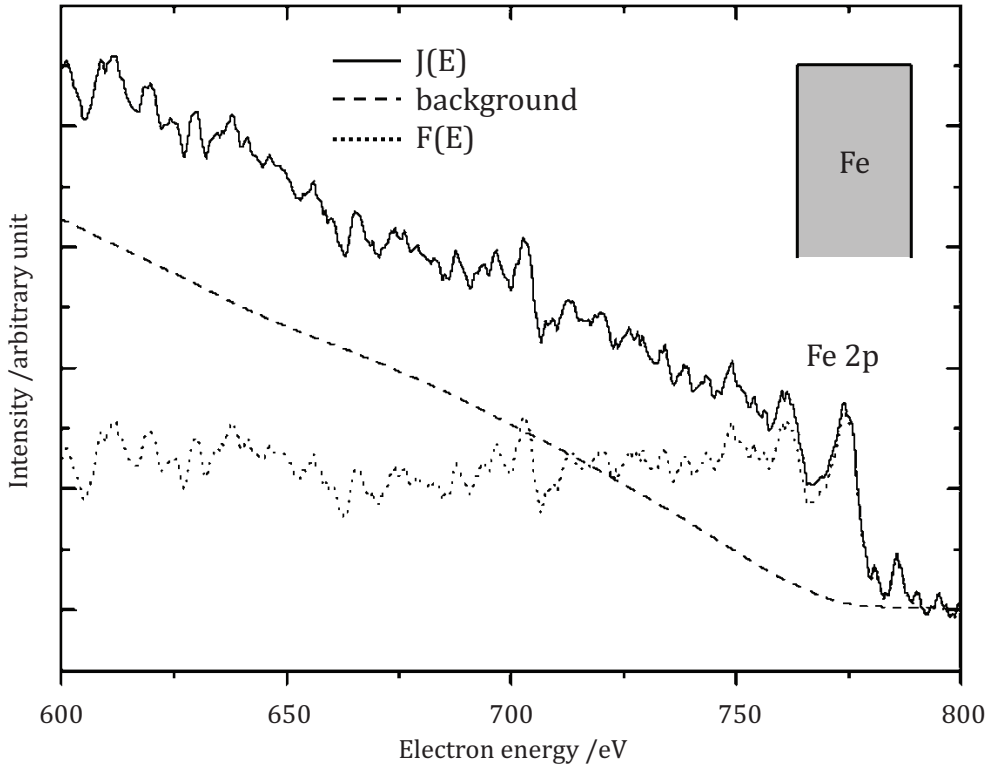

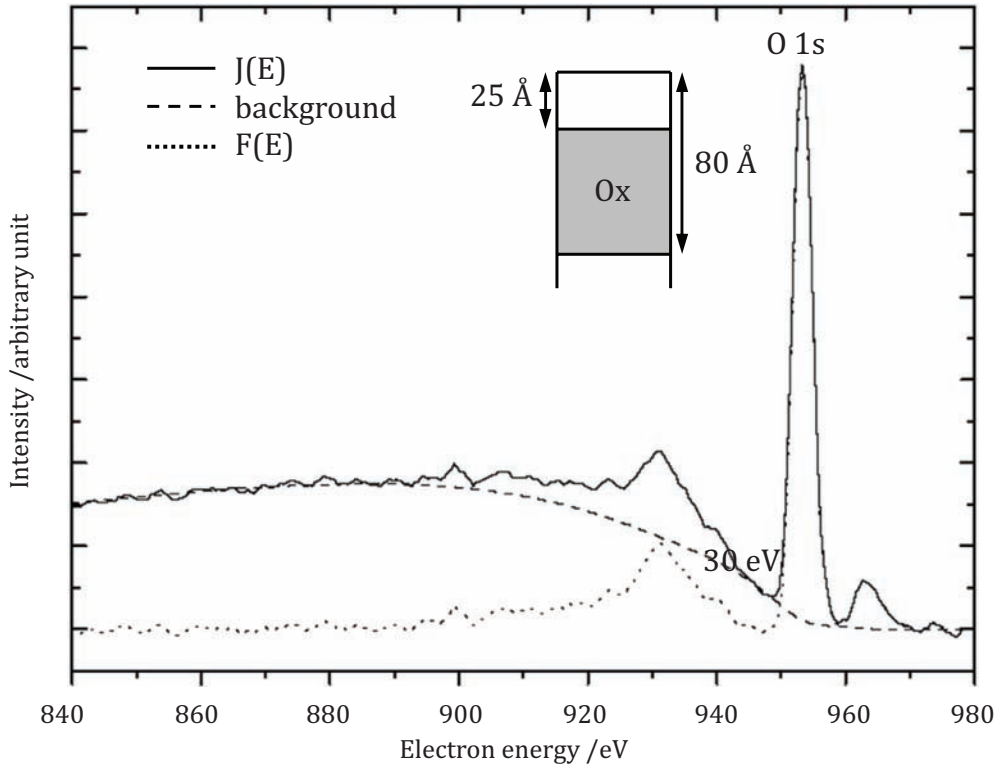

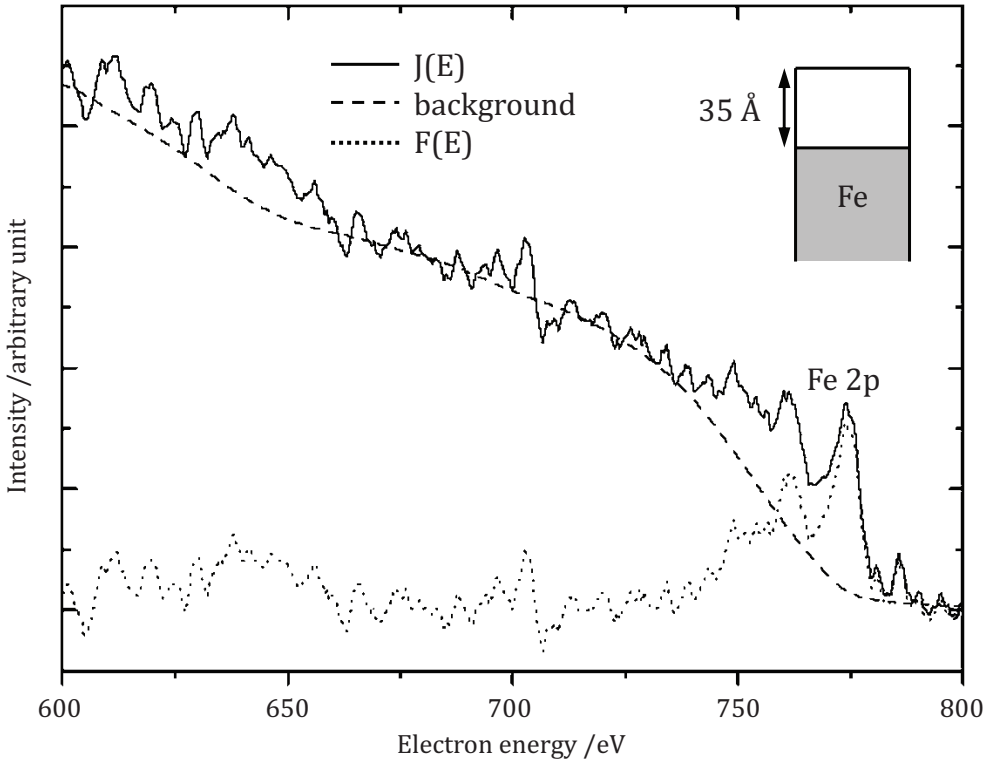

Figure C.6 — Spectra from the Fe sample of Figure C.2 that had been exposed to a maritime environment. The Fe 2p and O 1s peaks have been analysed with the Quases-Tougaard software[85] to determine the depth distributions of the O and Fe atoms[85]

Annex D
(informative)

XPS with sputter-depth profiling

D.1 Introduction

The method of sputter-depth profiling with XPS gives the in-depth distribution of elemental or compound composition of thin films. This Annex provides guidance on this method and gives an example.

By bombarding a solid surface with energetic ions, the outermost layer is removed and the underlying layer becomes the new surface. By repeating ion sputtering and XPS measurement in turn, the intensities of photoelectron peaks identified as arising from particular elements or compounds can be measured as a function of sputtering time.

D.2 Parameters for sputter-depth profiling

The alignment of the ion beam on the sample is most important and ISO 14606[108] gives guidance on procedures for alignment.

The following important factors should be considered when a high-depth-resolution profile is required.

a) use of low-energy Ar ions (<1 000 eV) and high incident angles (>60° from the surface normal) for metals and inorganic materials in order to reduce atomic mixing;

b) use of C_{60} or Ar^+ cluster ions for organic materials;

c) use of sample rotation during ion sputtering in order to reduce development of ion-induced surface roughness;

d) use of a high-spatial-resolution mode (<100 μm), if available, for the XPS measurements to avoid broadening of the depth profiles due to possible lateral inhomogeneities of the sample (e.g. edge effects).

NOTE Use of the Logistic Function Profile Fitting program[111] or the mixing-roughness-information depth model[112] is recommended to determine the depth resolution in a measured profile.

D.3 Example of XPS with sputter-depth profiling

Figures D.1 and D.2 show an example of XPS with sputter-depth profiling for an organic thin film (wax on polyurethane).[113] The surface regions of most organic specimens are easily damaged by energetic ion bombardment. It is thus important to sputter with low-energy ions. The depth profiles in Figures D.1 and D.2 were obtained with a 10 keV C_{60} cluster ion beam. The kinetic energy of each carbon ion that is produced on collision with the specimen surface is reduced to 1/60 of the primary-beam energy

The sputter-depth profiles displayed in Figure D.2 show the presence of a 10 nm to 15 nm surface layer that is C rich and depleted in N and O. Figure D.1 shows that the C 1s spectra for the surface layer have a different intensity distribution than the spectra for the polyurethane substrate.

The XPS data consist of measurements of photoelectron intensity for particular peaks as a function of sputtering time. The objective of sputter-depth profiling is to determine the quantitative concentration of elements or compounds as a function of depth. The ions collide with the surface and interact with atoms and electrons in the target material. These interactions are described in many published

papers. [114] [115] [116] A depth profile is said to be calibrated when surface composition is derived from the intensity data and sputtered depth is derived from sputtering time.

NOTE The sputtering time can be converted to sputtered depth from a measurement of sputtering rate of the sample material. The profile of the sputter crater is measured with a surface profilometer, as described in ISO 14606[117] and ISO/TR 15969.[118]

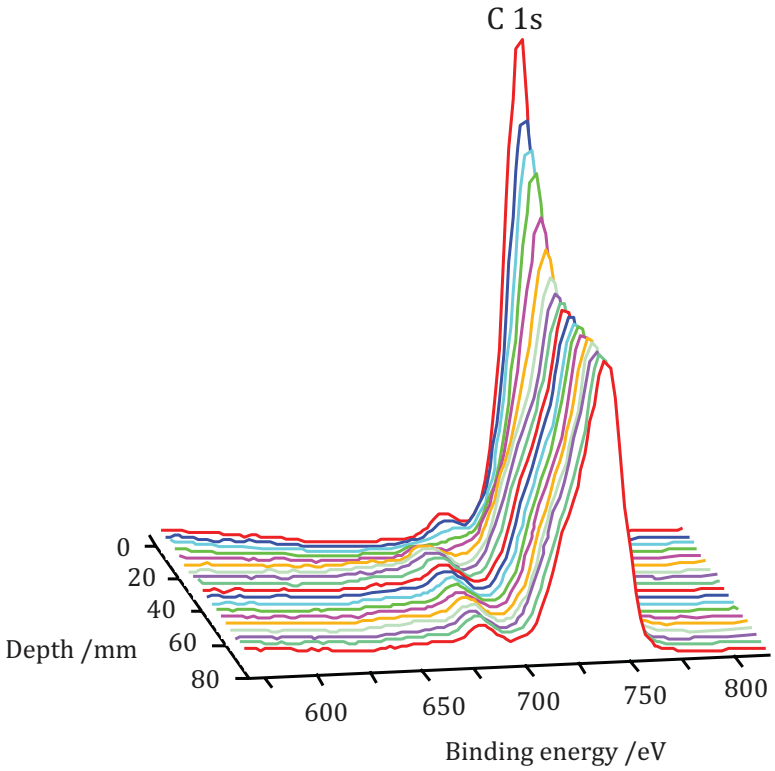

Figure D.1 — C 1s spectra from the C_{60} sputter-depth profile show the presence of a thin wax layer on the surface of the polyurethane sample

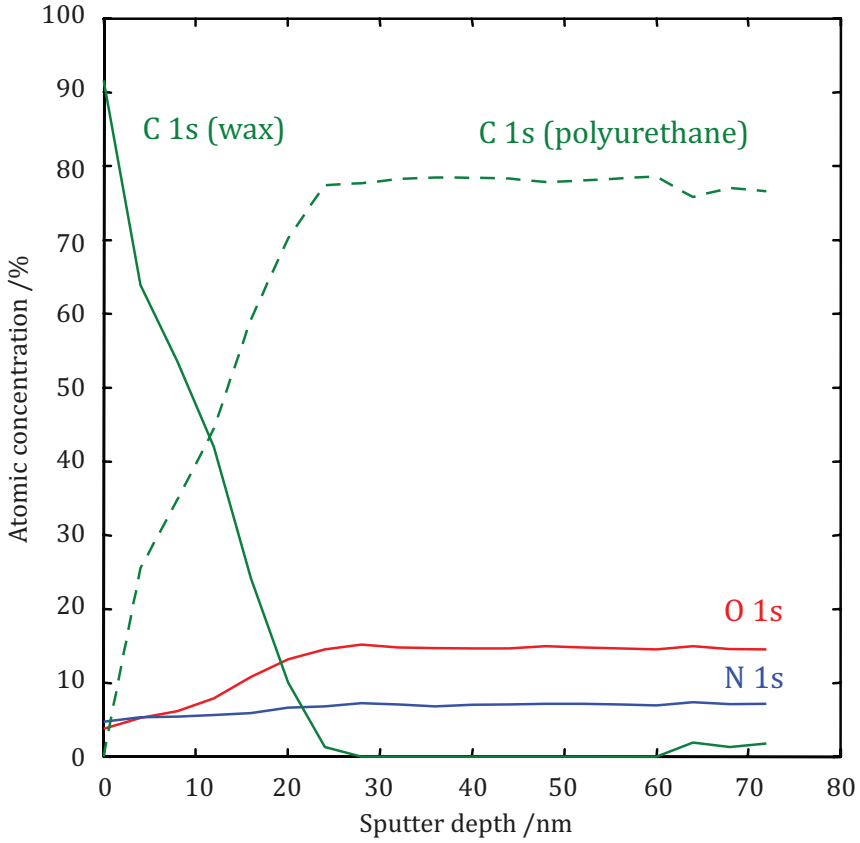

Figure D.2 — Chemical-state depth profile, showing the presence of a thin wax layer on the surface of the polyurethane sample

Bibliography

[1] Electron Effective-Attenuation-Length Database N.I.S.T. *SRD 82, Version 1.3*. National Institute of Standards and Technology, Gaithersburg, USA, 2011

[2] Jablonski A., & Powell C.J. Practical Expressions for the Mean Escape Depth, the Information Depth, and the Effective Attenuation Length in Auger-Electron Spectroscopy and X-ray Photoelectron Spectroscopy, *Journal of Vacuum Science and Technology A*, March/April 2009, **27** pp. 253-261

[3] Czanderna A.W., Madey T.E., Powell C.J.eds. *Beam Effects, Surface Topography, and Depth Profiling in Surface Analysis*. Plenum Press, New York, 1998

[4] Pijolat M.M., & Hollinger G. New depth-profiling method by angular-dependent X-ray photoelectron spectroscopy. *Surf. Sci.* 1981 April, **105** pp. 114–120

[5] Tougaard S. Surface nanostructure determination by X-ray photoemission spectroscopy peak shape analysis. *J. Vac. Sci. Technol. A*. 1996 May, **14** pp. 1415–1423

[6] Lysaght P.S., Barnett J., Bersuker G.I., Woicik J.C., Fischer D.A., Foran B., Tseng H.-H., Raj J. Chemical analysis of HfO2/Si(100) film systems exposed to NH3 thermal processing, *Journal of Applied Physics*, January 2007, **101**, art. 024105, pp 1-9

[7] Miyayama T., Sanada N., Bryan S.R., Hammond J.S., Suzuki M. Removal of Ar^+ beam-induced damaged layers from polyimide surfaces with argon gas cluster ion beams. *Surf. Interface Anal.* 2010 July, **42** pp. 1453–1457

[8] Sanada N., Yamamoto A., Oiwa R., Ohashi Y. Extremely low sputtering degradation of polytetrafluoroethylene by C_{60} ion beam applied in XPS analysis. *Surf. Interface Anal.* 2004 June, **36** pp. 280–282

[9] Sakai D., Sanada N., Hammond J.S., Iwai H. Recent Developments and Applications in AES and XPS. *J. Surf. Anal.* 2005 March, **12** pp. 97–100. Available at: <http://www.sasj.jp/JSA/CONTENTS/jsa_list.html>

[10] ISO 18116, *Surface chemical analysis — Guidelines for preparation and mounting of specimens for analysis*

[11] ISO 18117, *Surface chemical analysis — Handling of specimens prior to analysis*

[12] ISO 15472, *Surface chemical analysis — X-ray photoelectron spectrometers — Calibration of energy scales*

[13] ISO 24237, *Surface chemical analysis — X-ray photoelectron spectroscopy — Repeatability and constancy of intensity scale*

[14] ISO 21270, *Surface chemical analysis — X-ray photoelectron and Auger electron spectrometers — Linearity of intensity scale*

[15] ISO 19318, *Surface chemical analysis — X-ray photoelectron spectroscopy — Reporting of methods used for charge control and charge correction*

[16] Swift P. Adventitious Carbon — The Panacea for Energy Referencing? *Surf. Interface Anal.* 1982 April, **4** pp. 47–57

[17] Tanuma S., Powell C.J., Penn D.R. Calculations of electron inelastic mean free paths. V. Data for 14 organic compounds over the 50-2000 eV range. *Surf. Interface Anal.* 1994 September, **21** pp. 165–176

[18] Jablonski A., & Powell C.J. Evaluation of correction parameters for elastic-scattering effects in X-ray photoelectron spectroscopy and Auger electron spectroscopy. *J. Vac. Sci. Technol. A*. 1997 July, **15** pp. 2095–2106

[19] Toyoda S., Kumigashira H., Oshima M., Liu G.L., Liu Z., Ikeda K. In-Depth Profile of Hf-Based Gate Insulator Films on Si Substrates Studied by Angle-Resolved Photoelectron Spectroscopy Using Synchrotron Radiation. *Journal of Surface Analysis*. 2009 March, **15** pp. 299-302, http://www.sasj.jp/JSA/CONTENTS/jsa_list.html

[20] ISO 16243, *Surface chemical analysis - Recording and reporting data in X-ray photoelectron spectroscopy (XPS)*

[21] Seah M.P. Quantification in AES and XPS. In: *Surface Analysis by Auger and X-ray Photoelectron Spectroscopy*, (Briggs D., & Grant J.T.eds.). IM Publications and Surface Spectra Limited, 2003, pp. 345–75

[22] ISO 20903, *Surface chemical analysis — Auger electron spectroscopy and X-ray photoelectron spectroscopy — Methods used to determine peak intensities and information required when reporting results*

[23] Powell C.J., & Jablonski A. *NIST Inelastic-Mean-Free-Path Database, Version 1.2, Standard Reference Data Program Database 71* US Department of Commerce, National Institute of Standards and Technology Gaithersburg, MD, 2010, http://www.nist.gov/srd/nist71.cfm

[24] Jablonski A., Salvat F., Powell C.J. *NIST Electron Elastic-Scattering Cross-Section Database, Version 3.2, Standard Reference Data Program Database 64*. US Department of Commerce, National Institute of Standards and Technology, Gaithersburg, MD, 2010, http://www.nist.gov/srd/nist64.cfm

[25] Elastic Scattering of Electrons and Positrons. ICRU Report 77, Journal of the ICRU, vol. 7 International Commission on Radiation Units and Measurements. Oxford University Press, Oxford, 2007

[26] Salvat F., Jablonski A., Powell C.J. ELSEPA—Dirac partial-wave calculation of elastic scattering of electrons and positrons by atoms, positive ions and molecules. *Comput. Phys. Commun.* 2005, **165** pp. 157–190

[27] Jablonski A., & Powell C.J. Improved algorithm for calculating transport cross sections of electrons with energies from 50 eV to 30 keV. *Phys. Rev. B*. 2007 August, **76** p. 085123

[28] Hill M., Royce D.G., Fadley C.S., Wagner L.F., Grunthaner F.J. Properties of oxidized silicon as determined by angular-dependent X-ray photoelectron spectroscopy. *Chem. Phys. Lett.* 1976 December, **44** pp. 225–231

[29] Tanuma S. Electron Attenuation Lengths. In: *Surface Analysis by Auger and X-ray Photoelectron Spectroscopy*, (Briggs D., & Grant J.T.eds.). IM Publications and Surface Spectra Limited, 2003, pp. 259–94

[30] Jablonski A., & Powell C.J. The electron attenuation length revisited. *Surf. Sci. Rep.* 2002 June, **47** pp. 33–91

[31] *ISO/TR 18392: Surface chemical analysis - photoelectron spectroscopy - Procedures for determining backgrounds*. International Organization for Standardization, Genève, Switzerland, 2005

[32] ISO 18118, *Surface chemical analysis — Auger electron spectroscopy and X-ray photoelectron spectroscopy — Guide to the use of experimentally determined relative sensitivity factors for the quantitative analysis of homogeneous materials*

[33] Seah M.P. Simple Method of Depth Profiling (Stratifying) Contamination Layers, Illustrated by Studies on Stainless Steel, *Surface and Interface analysis*, June - July 1994, **21** pp 336–341

[34] Iwai H., Hammond J.S., Tanuma S. Recent Status of Thin Film Analyses by XPS. *J. Surf. Anal.* 2009 March, **15** pp. 264–270. Available at: <http://www.sasj.jp/JSA/CONTENTS/jsa_list.html>

[35] Cumpson P.J. The Thickogram: a method for easy film thickness measurement in XPS. *Surf. Interface Anal.* 2000 June, **29** pp. 403–406

[36] TBJ0801: Ultra Thin Film Analysis – structure analysis, Technical Bulletin, ULVAC-PHI INC., January 2008

[37] Seelmann-Eggebert M., & Keller R.C. Information on compositional depth profiles conveyed by angle-resolved XPS. *Surf. Interface Anal.* 1995 August, **23** pp. 589–600

[38] Bussing T.D., & Holloway P.H. Deconvolution of concentration depth profiles from angle resolved X-ray photoelectron spectroscopy data. *J. Vac. Sci. Technol. A*. 1985, **3** pp. 1973–1981

[39] Nefedov V.I., & Baschenko O.A. Relative intensities in ESCA and quantitative depth profiling. *J. Electron Spectrosc. Relat. Phenom.* 1988 February, **47** pp. 1–25

[40] Hazell L.B., Brown I.S., Freisinger F. A model for determining the composition of layer structured samples using XPS electron take-off angle experiments. *Surf. Interface Anal.* 1986 February, **8** pp. 25–31

[41] Ro C. Simulation study on regeneration of depth profiles from angle-resolved XPS data. *Surf. Interface Anal.* 1997 October, **25** pp. 869–877

[42] Cumpson P.J. Angle-resolved XPS and AES: Depth-resolution limits and a general comparison of properties of depth-profile reconstruction methods. *J. Electron Spectrosc. Relat. Phenom.* 1995 May, **73** pp. 25–52

[43] Jisl R. Restoration of the depth-concentration profile from the angle-resolved relative intensities of X-ray photoelectron spectra. *Surf. Interface Anal.* 1990 December, **15** pp. 719–726

[44] Tyler B.J., Castner D.G., Ratner, B.D. Regularization: A stable and accurate method for generating depth profiles from angle-dependent XPS data. *Surf. Interface Anal.* 1989 August, **14** pp. 443–490

[45] Smith G.C., & Livesey A.K. Maximum entropy: A new approach to non-destructive deconvolution of depth profiles from angle-dependent XPS, *Surface and Interface Analysis*, June 1992, **19** pp. 175

[46] Livesey A.K., & Smith G.C. The determination of depth profiles from angle-dependent XPS using maximum entropy data analysis. *J. Electron Spectrosc. Relat. Phenom.* 1994 June, **67** pp. 439–461

[47] Grabherr M.G., Ebel H., Ebel M.F., Svagera R., Baron G. Investigation of concentration depth profiles by means of angle-resolved XPS: A polynomial model. *J. Electron Spectrosc. Relat. Phenom.* 1993 July, **63** pp. 43–52

[48] Yih R.S., & Ratner B.D. A comparison of two angular dependent ESCA algorithms useful for constructing depth profiles of surfaces. *J. Electron Spectrosc. Relat. Phenom.* 1987, **43** pp. 61–82

[49] Baschenko O.A., & Nefedov V.I. Depth profiling of elements in surface layers of solids based on angular resolved X-ray photoelectron spectroscopy. *J. Electron Spectrosc. Relat. Phenom.* 1990 September, **53** pp. 1–18

[50] Holloway P.H., & Bussing T.D. Quantitative surface analysis of layered materials, *Surface and Interface Analysis*, April 1992, **18**, pp. 251-256

[51] Paytner R.W. Modification of the Beer–Lambert equation for application to concentration gradients. *Surf. Interface Anal.* 1981 August, **3** pp. 186–187

[52] Childers D.G. *Modern Spectral Analysis*. IEEE Press, New York, 1978

[53] Smith G.C., & Livesey A.K. Maximum Entropy: a New Approach to Non-destructive deconvolution of Depth Profiles from Angle-dependent XPS, *Surface Interface Analysis*, June 1992, **19** pp. 175–180

[54] Tikhonov A.N., & Arsenin V.Y. *Solutions of Ill Posed Problems*. V.H. Winston and Sons, Washington, DC, January 1977

[55] Glasko V.B. *Inverse Problems of Mathematical Physics*. American Institute of Physics, New York, 1988

[56] Gull S.F., & Skilling J. IEE PROCEEDINGS–F, Communications. *Radar and Signal Processing*. 1984 October, **131** p. 646

[57] Kimura K., Nakajima K., Zhao M., Nohira H., Hattori T., Kobata M. et al. Combination of high-resolution RBS and angle-resolved XPS: accurate depth profiling of chemical states. *Surf. Interface Anal.* 2008, **40** pp. 423–426

[58] Merzlikin S.V., Tolkachev N.N., Strunskus T., Witte G., Glogowski T., Woll C. et al. Resolving the depth coordinate in photoelectron spectroscopy — Comparison of excitation energy variation vs. angular-resolved XPS for the analysis of a self-assembled monolayer model system. *Surf. Sci.* 2008, **602** pp. 755–767

[59] Brundle C.R., Conti G., Mack P. XPS and angle resolved XPS, in the semiconductor industry: Characterization and metrology control of ultra-thin films. *J. Electron Spectrosc. Relat. Phenom.* 2010 May, **178-179** pp. 433–448

[60] Osterwalder J. Structural Effects in XPS and AES: Diffraction. In: *Surface Analysis by Auger and X-ray Photoelectron Spectroscopy*, (Briggs D., & Grant J.T.eds.). IM Publications and Surface Spectra Limited, 2003, pp. 557–85.

[61] Grenet G., Jugnet Y., Homberg S., Poon H.C., DUC, T.M. Photoelectron diffraction and surface crystallography. *Surf. Interface Anal.* 1989 June, **14** pp. 367–375

[62] Seah M.P., & Spencer S.J. Ultrathin SiO2 on Si II. Issues in quantification of the oxide thickness. *Surf. Interface Anal.* 2002 August, **33** pp. 640–652

[63] Gries W.H. Angular intensity modulation in angle-resolved XPS and AES of non-crystalline ultrathin surface layers: The phenomenon and its implications. *Surf. Interface Anal.* 1991 October, **17** pp. 803–812

[64] Fulghum J.E., & Linton R.W. Quantitation of coverages on rough surfaces by XPS: An overview. *Surf. Interface Anal.* 1988 December, **13** pp. 186–192

[65] Ebel H., Ebel M.F., Fischer H., SchoßMann B., Svagera R. Experimental influences on the results of concentration depth profiling by ARXPS. *Surf. Interface Anal.* 1994 June-July, **21** pp. 490–498

[66] Werner W.S.M. Magic angle for surface roughness for intensity ratios in AES/XPS. *Surf. Interface Anal.* 1995 September, **23** pp. 696–704

[67] Powell C.J., & Jablonski A. Progress in quantitative surface analysis by X-ray photoelectron spectroscopy: Current status and perspectives. *J. Electron Spectrosc. Relat. Phenom.* 2010 May, **178-179** pp. 331–346

[68] Gunter P.L.J., Gilzeman O.L.J, Niemantsverdriet J.W. Surface roughness effects in quantitative XPS: magic angle for determining overlayer thickness. *Appl. Surf. Sci.* 1997 August, **115** pp. 342–346

[69] Zalm P. Overlayer corrections in XPS. *Surf. Interface Anal.* 1998 May, **26** pp. 352–35

[70] Kappen P., Reihs K., Seidel C., Voetz M., Fuchf H. Overlayer thickness determination by angular dependent X-ray photoelectron spectroscopy (ADXPS) of rough surfaces with a spherical topography. *Surf. Sci.*, October 2000, vol. 465, pp. 40-50

[71] Olejnik K., Zemek J., Werner W.S.M. Angular-resolved photoelectron spectroscopy of corrugated surfaces. *Surf. Sci.*, 2005 December, **595** pp. 212–222

[72] Zemek J., Olejnik K., Klapetek P. Photoelectron spectroscopy from randomly corrugated surfaces. *Surf. Sci.*, 2008 April, **602** pp. 1440–1446

[73] Cumpson P.J.In: *Angle-Resolved X-ray Photoelectron Spectroscopy in Surface Analysis by Auger and X-ray Photoelectron Spectroscopy*. (Briggs D., & Grant J.T.eds.). IM Publications and Surface Spectra Limited, 2003, pp. 651–75

[74] Powell C.J., Jablonski A., Tilinin S., Tanuma S., Penn D.R. Surface sensitivity of Auger-electron spectroscopy and X-ray photoelectron spectroscopy. *J. Electron Spectrosc. Relat. Phenom.* 1999 January, **98-99** pp. 1–15

[75] Powell C.J., Werner W.S.M., Smekal W. Distinguishability of N composition profiles in SiON films on Si by angle-resolved X-ray photoelectron spectroscopy, *Applied Physics Letters*, October 2006, **89** pp. 172101-1–172101-3

[76] Tougaard S. Composition depth information from the inelastic background signal in XPS. *Surf. Sci.* 1985 October, **162** pp. 875–885

[77] Tougaard S. Inelastic background removal in X-ray excited photoelectron spectra from homogeneous and inhomogeneous solids. *J. Vac. Sci. Technol. A*. 1987 July, **5** pp. 1230–1234

[78] Tougaard S. Quantitative analysis of the inelastic background in surface electron spectroscopy. *Surf. Interface Anal.* 1988 June, **11** pp. 453–472

[79] Tougaard S., & Hanssen H.S. Non-destructive depth profiling through quantitative analysis of surface electron spectra. *Surf. Interface Anal.* 1989 November, **14** pp. 730–738

[80] Tougaard S. Accuracy of the non-destructive surface nanostructure quantification technique based on analysis of the XPS or AES peak shape. *Surf. Interface Anal.* 1998 April, **26** pp. 249–269

[81] Tougaard S.In: *Quantification of Nano-structures by Electron Spectroscopy in Surface Analysis by Auger and X-ray Photoelectron Spectroscopy*. (Briggs D., & Grant J.T.eds.). IM Publications and Surface Spectra Limited, 2003, pp. 295–343

[82] Tougaard S. Low energy inelastic electron scattering properties of noble and transition metals. *Solid State Commun.* 1987 September, **61** pp. 547–549

[83] Tougaard S. Universality Classes of Inelastic Electron Scattering Cross-sections. *Surf. Interface Anal.* 1997 March, **25** pp. 137–154

[84] Tanuma S., Powell C.J., Penn D.R. Calculation of electron inelastic mean free paths (IMFPs) VII. Reliability of the TPP-2M IMFP predictive equation. *Surf. Interface Anal.* 2003 March, **35** pp. 268–275

[85] Tougaard S. QUASES: Software package for Quantitative XPS/AES of Surface Nanostructure by Peak Shape Analysis, **5.1** (2002-2005). See at http://www.quases.com/

[86] Tougaard S. X-ray photoelectron spectroscopy peak shape analysis for the extraction of in-depth composition information. *J. Vac. Sci. Technol. A*. 1987 July, **5** pp. 1275–1278

[87] Johansson L.-S., Campbell J.M., Koljonen K., Kleen M., Buchert J. On surface distributions in natural cellulosic fibres. *Surf. Interface Anal.* 2004 August, **36** pp. 706–710

[88] Idala K., Johansson L.-S., Campbell J.M., Inganäs O. XPS and SIMS study: adhesion of polypyrrole film on titanium. *Surf. Interface Anal.* 2000 August, **30** pp. 557–560

[89] Tougaard S. Practical algorithm for background subtraction. *Surf. Sci.* 1989 June, **216** pp. 343–360

[90] Tougaard S. Formalism for quantitative surface analysis by electron spectroscopy. *J. Vac. Sci. Technol. A*. 1990 May, **8** pp. 2197–2203

[91] Tougaard S. Quantitative x-ray photoelectron spectroscopy: Simple algorithm to determine the amount of atoms in the outermost few nanometers. *J. Vac. Sci. Technol. A*. 2003 July, **21** pp. 1081–1086

[92] Tougaard S. Algorithm for automatic x-ray photoelectron spectroscopy data processing and x-ray photoelectron spectroscopy imaging. *J. Vac. Sci. Technol. A*. 2005 July, **23** pp. 741–745

[93] Hajati S., Tougaard S., Walton J., Fairley N. Noise reduction procedures applied to XPS imaging of depth distribution of atoms on the nanoscale. *Surf. Sci.* 2008 August, **602** pp. 3064–3070

[94] MultiPak AES & XPS Data Reduction Software Ver. 8.2C (2007) by ULVAC-PHI INC., 370 Enzo, Chigasaki, 253-8522, Japan. See <http://www.ulvac-phi.com/>

[95] Winters H.F., Graves D.B., Humbird D., Tougaard S. Penetration of fluorine into the silicon lattice during exposure to F atoms, F_2, and XeF_2: Implications for spontaneous etching reactions. *J. Vac. Sci. Technol. A*. 2007 January, **25** pp. 96–103

[96] Espinös J.P., Martin-Conceptión A.I., Mansilla C., Yubero F., González-Elipe A. R. X-ray photoelectron spectroscopy study of the nucleation processes and chemistry of CdS thin films deposited by sublimation on different solar cell substrate materials, *Journal of Vacuum Science and Technology A*, 2006, **24**, pp. 919-928

[97] Zhou M., Wu C., Edirisinghe D., Drummond J.L., Hanley L. Organic overlayer model of a dental composite analysed by laser desorption postionization mass spectrometry and photoemission. *J. Biomed. Mater. Res.* 2006 April, **77A** pp. 1–10

[98] Eon D., Cartry G., Fernandez V., Cardinaud C., Tegou E., Bellas V. et al. Surface segregation of photoresist copolymers containing polyhedral oligomeric silsesquioxanes studied by x-ray photoelectron spectroscopy. *J. Vac. Sci. Technol. B*. 2004 September/October, **22** pp. 2526–2532

[99] Garcia F., Yubero F., Espinös J.P., Gonzalez-Elipe A.R. First nucleation steps of vanadium oxide thin films studied by XPS inelastic peak shape analysis. *Appl. Surf. Sci.* 2005 September, **252** pp. 189–195

[100] Johansson E., & Nyborg L. XPS study of carboxylic acid layers on oxidized metals with reference to particulate materials. *Surf. Interface Anal.* 2003 April, **35** pp. 375–381

[101] Zemek J., Jiricek P., Jablonski A., Lesiak B. Growth mode of ultrathin gold films deposited on nickel. *Appl. Surf. Sci.* 2002 October, **199** pp. 138–146

[102] Fuoco E.R., & Hanley L. Large fluorocarbon ions can contribute to film growth during plasma etching of silicon. *J. Appl. Phys.* 2002 July, **92** pp. 37–44

[103] Re M.D., Gouttebaron R., Dauchot J.P., Leclëre P., Lazzaroni R., Wautelet M. et al. Growth and morphology of magnetron sputter deposited silver films. *Surf. Coat. Tech.* 2002 March, **151-152** pp. 86–90

[104] Mansilla C., Gracia F., Martin-Conceptión A.I., Espinös J.P., Holgado J.P., Yubero F. et al. Study of the first nucleation steps of thin films by XPS inelastic peak shape analysis. *Surf. Interface Anal.* 2007 April, **39** pp. 331–336

[105] Hajati S., Zaporojtchenko V., Faupel F., Tougaard S. Characterization of Au nano-cluster formation on and diffusion in polystyrene using XPS peak shape analysis. *Surf. Sci.* 2007 August, **601** pp. 3261–3267

[106] Tougaard S. Inelastic background correction and quantitative surface analysis. *J. Electron Spectrosc. Relat. Phenom.* 1990, **52** pp. 243–271

[107] Tougaard S., & Sigmund P. Influence of elastic and inelastic scattering on energy spectra of electrons emitted from solids. *Physicals Review B*. 1982 April, **25** pp. 4452–4466

[108] Landau L. Energy loss of fast particles by ionization. *J. Phys.* 1944, **8** pp. 201–205 [Moscow]

[109] Simonsen A.C., Schleberger M., Tougaard S., Hansen J.L., Nylandsted-Larsen A. Nanostructure of Ge deposited on Si(001): a study by XPS peak shape analysis and AFM. *Thin Solid Films*. 1999 January, **338** pp. 165–171

[110] Hansen H.S., & Tougaard S. Separation of spectral components and depth profiling through inelastic background analysis of XPS spectra with overlapping peaks. *Surf. Interface Anal.* 1991 July, **17** pp. 593–607

[111] http://www.nist.gov/mml/surface/lfpf.cfm

[112] Hofmann S. Ultimate depth resolution and profile reconstruction in sputter profiling with AES and SIMS. *Surf. Interface Anal.* 2000, **30** pp. 228–236

[113] Thin Film Analysis of Polymer Additive Migration Using the PHI Model 06-C60 Sputter Ion Gun, Application Note, Physical Electronics USA, 2007

[114] Smith R. Atom and Ion Collisions in Solids and Surfaces, Cambridge University Press, Cambridge, UK, January 1997, pp. 1-319

[115] Behrisch R.In: *Sputtering by Ion Bombardment: Theoretical Concept in Sputtering by Particle Bombardment II*. (Behrisch R.ed.). Topics in Applied Physics. Springer Berlin, Germany, **Vol. 52**, 1983

[116] Malherbe J.B. Sputtering of compound semiconductor surfaces. II. Compositional changes and radiation-induced topography and damage. *CRC Critical Reviews in Solid State and Materials Science*. 1994, **19** pp. 129–195

[117] ISO 14606, *Surface chemical analysis — Sputter depth profiling — Optimization using layered systems as reference materials*

[118] ISO/TR 15969: *Surface chemical analysis – Depth profiling – Measurement of sputtered depth*

ICS 71.040.40

Price based on 46 pages